nature cell biology

Direct inhibition of the cold-activated TRPM8 ion channel by $G\alpha_q$

Xuming Zhang[1,3], Stephanie Mak[1], Lin Li[1], Andres Parra[2], Bristol Denlinger[2], Carlos Belmonte[2] and Peter A. McNaughton[1,3]

Activation of the TRPM8 ion channel in sensory nerve endings produces a sensation of pleasant coolness. Here we show that inflammatory mediators such as bradykinin and histamine inhibit TRPM8 in intact sensory nerves, but do not do so through conventional signalling pathways. The G-protein subunit $G\alpha_q$ instead binds to TRPM8 and when activated by a Gq-coupled receptor directly inhibits ion channel activity. Deletion of $G\alpha_q$ largely abolished inhibition of TRPM8, and inhibition was rescued by a $G\alpha_q$ chimaera whose ability to activate downstream signalling pathways was completely ablated. Activated $G\alpha_q$ protein, but not $G\beta\gamma$, potently inhibits TRPM8 in excised patches. We conclude that $G\alpha_q$ pre-forms a complex with TRPM8 and inhibits activation of TRPM8, following activation of G-protein-coupled receptors, by a direct action. This signalling mechanism may underlie the abnormal cold sensation caused by inflammation.

The temperature-sensitive ion channels TRPV1 and TRPM8 play an essential role in pain. Inflammatory mediators released during tissue injury or inflammation enhance heat pain by sensitizing the heat-gated TRPV1 ion channel through intracellular signalling pathways whose end point is phosphorylation of TRPV1 by protein kinases[1–5]. The TRPM8 ion channel is activated by cold temperatures[6,7], and is also involved in many aspects of pain sensation such as cold analgesia, and paradoxically cold hypersensitivity[8–12]. Acute activation of TRPM8, by cooling or by application of agonists of TRPM8 such as menthol, causes an analgesic effect[8,9]. Cold hypersensitivity, on the other hand, is observed in chronic inflammatory conditions, and increased TRPM8 expression seems to be an underlying mechanism[8,10,13]. It is thus unclear how TRPM8-expressing cold thermoreceptors may be affected by inflammation.

The membrane PIP_2 level regulates TRPM8 activity. TRPM8 activity increased when PIP_2 was applied to the intracellular surface of excised patches[14,15], and was reduced when membrane PIP_2 was depleted[16]. A decrease in membrane PIP_2, caused by activation of the PLC pathway following binding of an agonist such as bradykinin (BK) to a Gq-coupled G-protein-coupled receptor (GPCR), was therefore assumed to be responsible for inhibiting TRPM8 channel activity[14,15]. However, other studies have proposed that PKC is instead involved in the inhibition of TRPM8 by BK (refs 17,18).

In the present study we examined the effect of inflammatory mediators on TRPM8-dependent nerve activity, and we confirm that TRPM8 is inhibited by inflammatory mediators that couple to $G\alpha_q$. However, we found that the inhibition of TRPM8 activity is largely independent of cell signalling pathways downstream of $G\alpha_q$-coupled receptors. Neither depletion of membrane PIP_2 nor phosphorylation by PKC is crucial. Instead we found that activated $G\alpha_q$ binds to TRPM8, and causes inhibition by a direct action following activation of $G\alpha_q$-coupled receptors.

RESULTS

Inflammation inhibits TRPM8-dependent cold nerve fibre activity

Cold-sensitive fibres innervating the cornea of the eye detect small changes in ambient cold temperature, a property solely dependent on TRPM8 channel expression[19]. We first examined the effect of inflammatory mediators on cold-sensitive fibres of the cornea. A cooling ramp from 34 to 20 °C elicited an increasing discharge of nerve impulses (Fig. 1a), known to be attributable to activation of TRPM8 (ref. 19). A heat ramp to 48 °C initially suppressed ongoing TRPM8-dependent activity, but then reactivated firing at 45 °C, probably because of heat-dependent activation of TRPV1. However, when an 'inflammatory soup', containing BK and histamine was perfused, increases in firing frequency evoked by cooling were smaller

[1]Department of Pharmacology, University of Cambridge, Tennis Court Road, Cambridge CB2 1PD, UK. [2]Instituto de Neurociencias de Alicante, Universidad Miguel Hernandez-Consejo Superior de Investigaciones Cientificas, 03550 San Juan de Alicante, Spain.
[3]Correspondence should be addressed to X.Z. or P.A.M. (e-mail: xz213@cam.ac.uk or pam42@cam.ac.uk)

Received 15 April 2012; accepted 22 May 2012; published online 1 July 2012; DOI: 10.1038/ncb2529

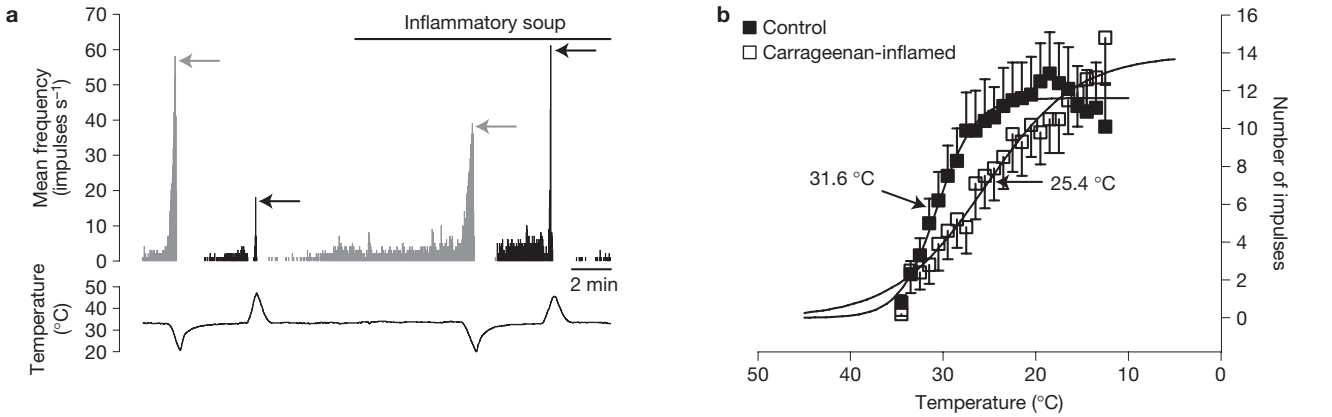

Figure 1 Inflammatory mediators inhibit TRPM8-dependent cold nerve fibre activity. (**a**) Corneal nerve terminal firing frequency in response to a cold ramp (grey bars) and a heat ramp (black bars). The bath temperature is shown below. Perfusion of inflammatory soup (5 μM BK, 100 μM histamine, 10 μM PGE2, 100 μM 5-HT and 100 μM ATP) inhibited the cold response (grey arrows) but enhanced the heat response (black arrows). The cold response recovered to control levels following removal of the inflammatory soup (not shown) but the heat response remained elevated. (**b**) Similar experiments on single afferent nerve fibres from the tongue. The vertical axis shows cumulative firing during a cold ramp. Filled squares, control ($n = 40$); open squares, tongue injected with carrageenan ($n = 32$, see Methods). All error bars are mean ± s.e.m.

(grey arrows in Fig. 1a, mean peak frequency before inflammatory soup perfusion, 44.3 ± 4.5 impulses per second; after inflammatory soup perfusion, 31.8 ± 3.4; $n = 12$, $P < 0.001$, paired t-test). A significantly larger temperature decrease (ΔT) for initiation of increased firing was also observed (ΔT before inflammatory soup perfusion, 1.1 ± 0.4 °C; after inflammatory soup perfusion, 1.8 ± 0.4 °C; $n = 12$, $P < 0.01$, paired t-test). In contrast, the firing frequency evoked by heat was enhanced by inflammatory mediators (black arrows, Fig. 1a). We found no significant desensitization of firing frequency under control conditions when saline solution was perfused[19] (mean peak frequency before saline solution perfusion, 47.5 ± 5.95 impulses per second; after saline perfusion, 44.0 ± 7.7; $n = 4$, $P > 0.05$, paired t-test; Supplementary Fig. S1a). These data show that inflammatory agents reduce TRPM8-mediated responses to cooling in intact cold thermoreceptor terminals *in situ*, while at the same time enhancing heat responses.

A similar result in cold-sensitive afferent nerve fibres of the mouse tongue was obtained when inflammation was induced by carrageenan injection. Figure 1b shows the cumulative sum of firing in single sensory afferent nerves as the temperature was lowered from 34 to 12 °C; the integral of firing as a function of temperature was half-activated at 31.6 ± 1.09 °C ($n = 40$) in control fibres but at 25.4 ± 0.81 °C ($n = 32$) in inflamed fibres.

Inflammatory mediators inhibit TRPM8 independently of conventional downstream signalling pathways

We next measured the activity of TRPM8 in cultured dorsal root ganglion (DRG) neurons by applying pulses of menthol, an agonist for TRPM8, and monitoring the rise in intracellular calcium caused by channel activation. In agreement with nerve fibre recordings, BK potently inhibited TRPM8 in 11 out of 33 TRPM8-positive neurons (Fig. 2a). PKC-mediated phosphorylation, either direct or through activation of a phosphatase, has been suggested to be responsible for inhibition of TRPM8 (refs 17,18), but we found that the BK-induced inhibition of TRPM8 was not abolished by the PKC inhibitor bisindolylmaleimide (BIM), and nor was it mimicked by the PKC activator phorbol 12-myristate 13-acetate (PMA; Fig. 2b and Supplementary Fig. S1b,c). Similar observations were made in HEK293 cells co-transfected with TRPM8 and the BK receptor B2R, in which BK inhibited TRPM8 with a similar efficacy to DRG neurons (Fig. 2c,d and Supplementary Fig. S1d). B2R-dependent inhibition of TRPM8 was not affected by the specific PKC inhibitor BIM, the broad PKC inhibitor staurosporine, the phosphatase inhibitor okadaic acid, nor the PLC inhibitor neomycin (Fig. 2d). Moreover, activation of PKC by PMA did not cause significant inhibition of TRPM8 (Fig. 2d), although PMA had a marked effect on TRPV1 (Supplementary Fig. S1e). These experiments do not favour the idea that signalling pathways downstream of PLC may underlie the effect of BK on TRPM8.

To extend these experiments, the current flowing through TRPM8 channels was monitored during voltage-clamp pulses to ±60 mV or in full I–V curves (Supplementary Fig. S2a,b), and the effects of inhibitors on signalling pathways were investigated. Membrane PIP_2 is known to activate TRPM8 (refs 14,15), and therefore PIP_2 hydrolysis following activation of PLCβ by G_q-coupled GPCRs could be a mechanism for inhibiting TRPM8. This idea is not supported, however, by the inability of U73122, a PLC inhibitor, to prevent the inhibition of TRPM8 currents (either inward or outward) caused by BK or histamine (Fig. 2e–h). The same concentration of U73122 completely inhibited PLC-mediated hydrolysis of PIP_2 and also inhibited the sensitization of TRPV1 induced by BK (Supplementary Fig. S3a,b), a process dependent on the PLC signalling pathway[5,20]. Moreover, histamine strongly inhibited TRPM8 currents in two PIP_2-insensitive TRPM8 mutants, K995Q and R1008Q (ref. 14; Fig. 2g,h). We also found that activation of PLCγ through application of nerve growth factor (NGF) had no inhibitory effect on TRPM8 (Fig. 2d, last bar). These experiments suggest that receptor-mediated hydrolysis of PIP_2 is not sufficient to inhibit TRPM8. A possible pathway involving activation of PLA_2 followed by coupling to $G\alpha_i$ is also not supported by the lack of effect of the PLA_2 inhibitor *N*-(*P*-amylcinnamoyl)anthranilic acid (ACA) and inactivation of $G\alpha_{i/o}$ by pertussis toxin (PTX; Fig. 2e,f). Disruption of intracellular Ca^{2+} signalling by applying the Ca uptake inhibitor thapsigargin, by buffering intracellular calcium with BAPTA-AM or by blocking the IP3 receptor with 2-APB also had no effect on BK-induced inhibition of TRPM8 currents, suggesting that intracellular Ca^{2+} release is not involved (Fig. 2f and Supplementary Fig. S1f).

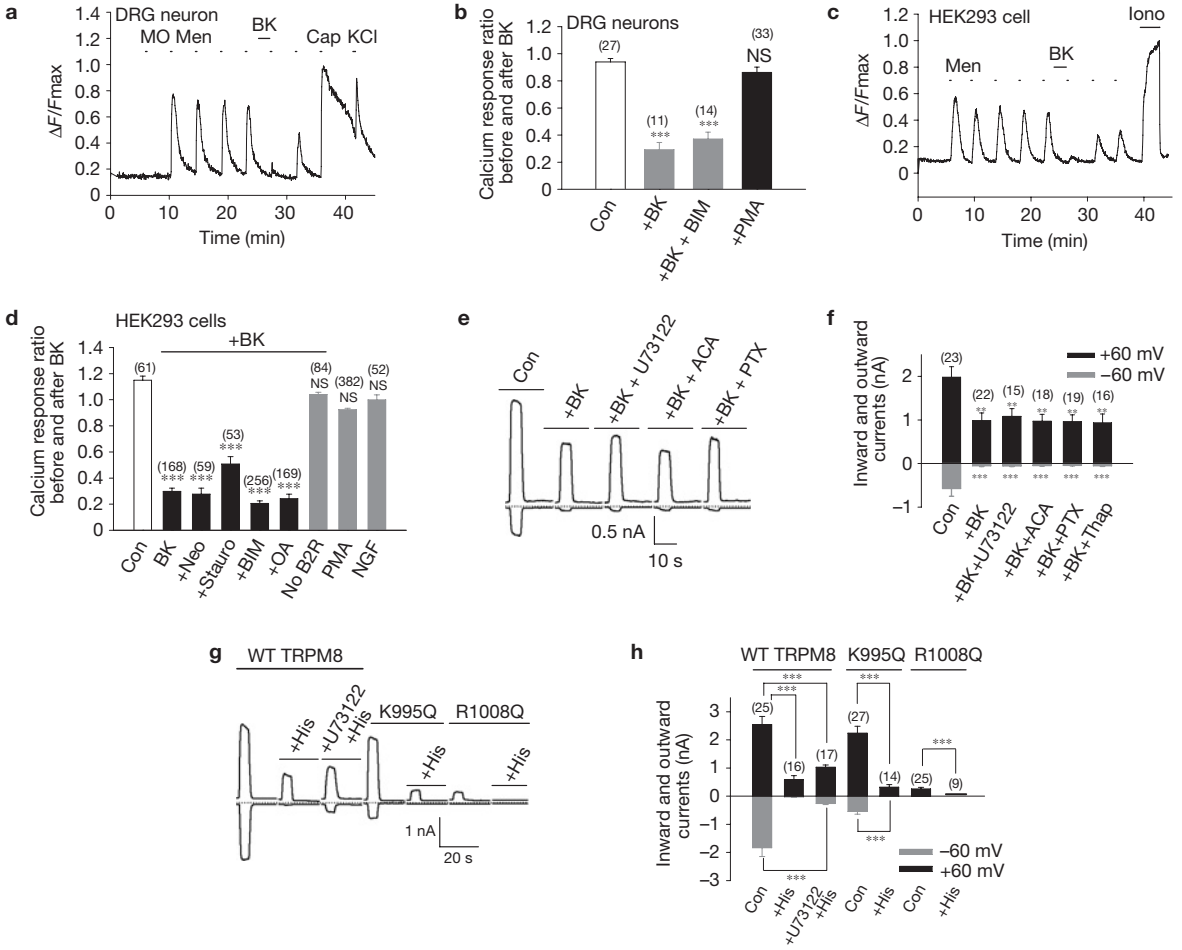

Figure 2 Inflammatory mediators inhibit TRPM8 independently of downstream signalling pathways. (**a**) BK (1 μM) inhibited the TRPM8-mediated calcium response in a DRG neuron responding to menthol (100 μM) and capsaicin (500 nM) but not mustard oil (MO, 50 μM), and thus expressing TRPM8 and TRPV1 but not TRPA1. KCl (140 mM) was added at the end. (**b**) A summary of the mean ratio of peak calcium responses to menthol before and after the application of BK alone (bar 2), as in **a**, or with BIM (1 μM; bar 3). Bars 2 and 3 show only BK-responsive neurons but inhibition was also significant when BK-unresponsive cells were included (Supplementary Fig. S1c). The final bar is a summary of experiments with PMA (see Supplementary Fig. S1b). The number of TRPM8-positive neurons is shown above each bar. (**c**) Ca increases elicited by menthol (100 μM), and effect of BK (1 μM) in a single HEK293 cell transfected with TRPM8 and B2R. The Ca ionophore ionomycin (Iono; 10 μM) was added at the end to saturate the Ca-dependent fluorescence signal. (**d**) A summary of results similar to those in **c** following treatment with neomycin (Neo, 1 mM), staurosporine (Stauro, 1 μM), BIM (1 μM), okadaic acid (OA, 20 nM) and PMA (1 μM) without BK. The final bar is from cells transfected with TRPM8 and TrkA receptor, and treated with NGF (100 ng ml^{-1}, 10 min). The number of cells is given above each bar. (**e**) Inward and outward currents (at −60 mV and +60 mV) activated by menthol (200 μM, 5 s) in HEK293 cells expressing TRPM8 and B2R were inhibited by pre-treatment with 1 μM BK (1 min) applied alone or together with inhibitors as indicated. The dotted line denotes zero current. (**f**) A summary of the peak currents in experiments similar to those in **e** following treatment with U73122 (2.5 μM), ACA (10 μM), PTX (1.0 μg ml^{-1}) and thapsigargin (Thap, 1 μM). The number of experiments is given above each bar. (**g**,**h**) Example (**g**) and summary (**h**) of inward and outward currents (±60 mV) in response to menthol application (200 μM, 5 s) in HEK293 cells expressing TRPM8 or mutants as shown together with H1R. Histamine (His, 10 μM) inhibits the TRPM8 current, and inhibition is little affected by 2.5 μM U73122 or by mutations reducing sensitivity to PIP_2. The dotted line is zero current. The number of experiments is given above each bar. All data are mean ± s.e.m., significance compared with control. $^{**}P < 0.01$; $^{***}P < 0.001$; NS, not significant.

Taken together, these data indicate that the conventional intracellular signalling pathways downstream of PLC are not involved in TRPM8 inhibition, and we therefore investigated other possible mechanisms.

Activated $G\alpha_q$ inhibits TRPM8 independently of the PLC pathway

Whether a diffusible intracellular mediator is involved in the inhibition of TRPM8 by BK can be determined by making cell-attached patch recordings of single channels and applying BK only outside the patch. Sensitization of TRPV1 depends on activation of kinases by the PLC signalling pathway[5], and as expected application of BK outside the patch potently enhanced channel activity (Fig. 3b). TRPM8 single-channel bursting, in contrast, was not inhibited by bath application of BK (Fig. 3a). These experiments suggest that BK-induced inhibition of TRPM8 is membrane-delimited and depends on local events within the patch, and not on diffusible messengers.

The local nature of TRPM8 channel inhibition suggested that activated $G\alpha_q$ itself may cause direct inhibition of TRPM8, as previously suggested for K channels[21,22]. $G\alpha_q$ has two forms, an inactive GDP-bound and an active GTP-bound form. Overexpression of $G\alpha_q$ had a small inhibitory effect on the TRPM8 inward current (Fig. 4a), presumably because a small proportion of $G\alpha_q$ is in the active GTP-bound form even in the absence of GPCR stimulation[23]. The $G\alpha_{q/11}$ Q209L

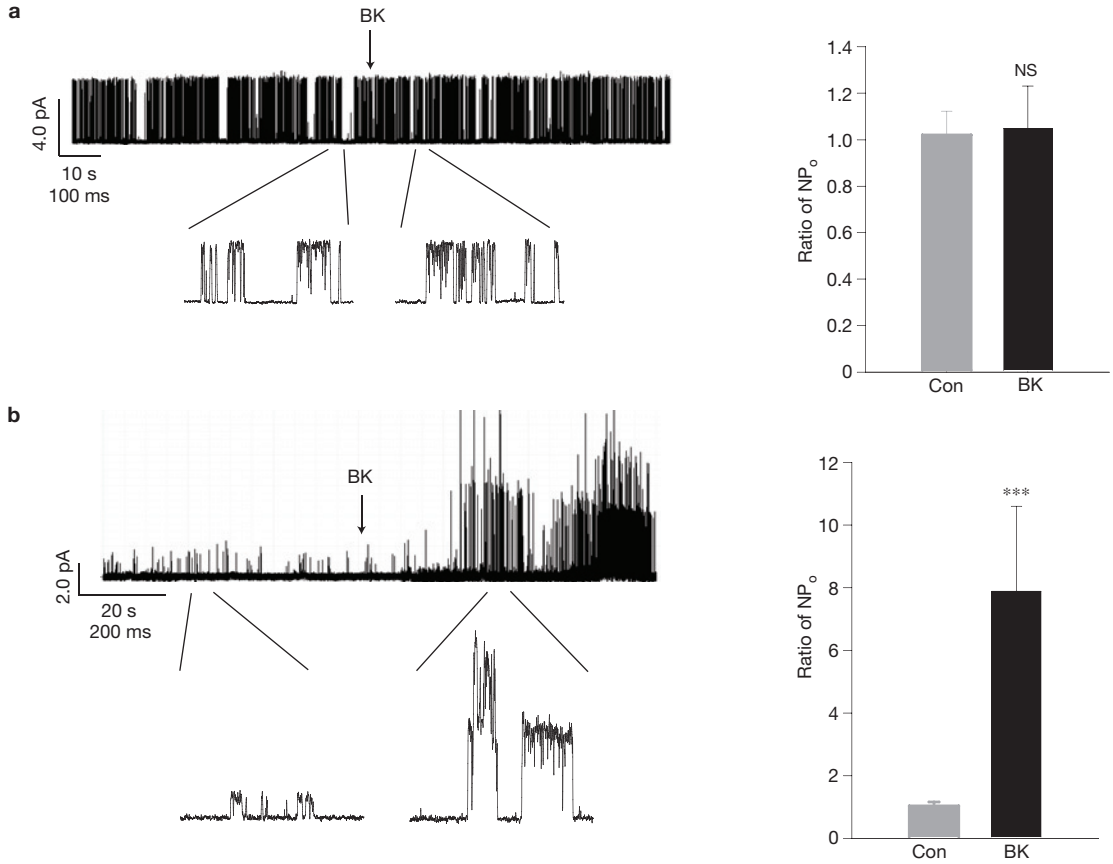

Figure 3 Inhibition of TRPM8 by BK is membrane-delimited. (**a**) A typical cell-attached recording of a single channel at +60 mV from HEK293 cells expressing TRPM8 and B2R. The arrow indicates the addition of 1 μM BK. Sections of traces are shown below at a higher time resolution (see the alternative scale bar on the left). Mean NP_o before BK addition, 0.13 ± 0.0092; after BK addition, 0.14 ± 0.0093; difference not significant, $P > 0.05$. On the right is a summary of the ratio of the mean NP_o before and after vehicle solution (Con) application, and before and after BK addition from the same patches. $n = 5$; NS, not significant. (**b**) A similar cell-attached recording performed at +40 mV on a HEK293 cell expressing TRPV1 and B2R. The patch contains multiple channels. Mean NP_o before BK addition, 0.01711 ± 0.0014; after BK addition, 0.1866 ± 0.0243; $P < 0.001$. On the right is a summary of the ratio of the mean NP_o before and after vehicle solution (Con) or BK addition in the same patches. Enhancement by BK significant, $^{***}P < 0.001$, $n = 5$. Error bars in all figures are mean ± s.e.m.

mutant, which is deficient in intrinsic GTPase activity and is therefore mainly in the GTP-bound active configuration[24], caused a much greater inhibition of both inward and outward TRPM8 currents (Fig. 4a,b).

Inhibition of TRPM8 by active $G\alpha_q$ could result from potent activation of PLCβ, and consequent hydrolysis of PIP_2. To investigate this possibility, we used a sensitive reporter of membrane PIP_2 levels, Tubby–R332H–cYFP (ref. 25), to monitor activation of the PLCβ/PIP_2 pathway. As expected, expression of the active mutant $G\alpha_q$ Q209L, which couples to PLCβ, caused complete translocation of Tubby to the cytoplasm, whereas wild-type $G\alpha_q$, which is largely in the inactive GDP-bound form, had no detectable effect (Supplementary Fig. S4a). A commonly used triple mutant $G\alpha_q$ Q209L/R256A/T257A, which has been reported to be unable to activate PLCβ (ref. 26), profoundly suppressed TRPM8 currents (Fig. 4b), but we found this mutant still caused substantial Tubby translocation (Supplementary Fig. S4a), and so in fact still couples to PLCβ. We therefore constructed a chimaera between $G\alpha_q$ and $G\alpha_{i2}$ by replacing the PLCβ-binding region on $G\alpha_q$ by the corresponding region on $G\alpha_{i2}$ (Fig. 6f). We found that this chimaera, which we named $3G\alpha_{qiq}$ (see below), completely failed to deplete PIP_2 even when made constitutively active by the Q209L mutation (Supplementary Fig. S4a). However, when activated by the Q209L mutation, $3G\alpha_{qiq}$ strongly inhibited both inward and outward TRPM8 currents (Fig. 4a,b), showing that the $3G\alpha_{qiq}$ chimaera retains the ability to couple to TRPM8, even though its coupling to PLCβ is selectively disabled. The inhibition of TRPM8 was specific to $G\alpha_q$, because other activated Gα subunits ($G\alpha_{i2}$ Q205L and $G\alpha_{13}$ Q226L) and $G\beta_1\gamma_2$ were without effect (Fig. 4b). Collectively, these experiments show that activated $G\alpha_q$ can directly inhibit TRPM8, independently of the downstream PLC pathway.

The effect of $G\alpha_q$ on TRPM8 inward currents activated by menthol is shown in Fig. 4c. Overexpression of $G\alpha_q$ reduced TRPM8 sensitivity to menthol, because a small fraction is in the active GTP-bound conformation (see above). The constitutively active but signalling-ablated mutant $3G\alpha_{qiq}$ Q209L caused a stronger inhibition of TRPM8 sensitivity to menthol. Conversely, expression of TRPM8 in mouse embryonic fibroblast (MEF) cells lacking endogenous $G\alpha_{q/11}$ (ref. 27) enhanced TRPM8 sensitivity to menthol, showing that endogenous $G\alpha_q$ imposes a tonic inhibition on TRPM8. Outward TRPM8 currents can be evoked by strong depolarization in either the absence or presence of menthol, and these currents were suppressed by $G\alpha_q$ and to an even greater extent by $3G\alpha_{qiq}$ Q209L, leading to a shift of the G–V curve and a significant positive shift in $V_{1/2}$ (Fig. 4d–f). We noticed that currents recorded in cells without menthol consistently have a larger noise than in the presence of menthol,

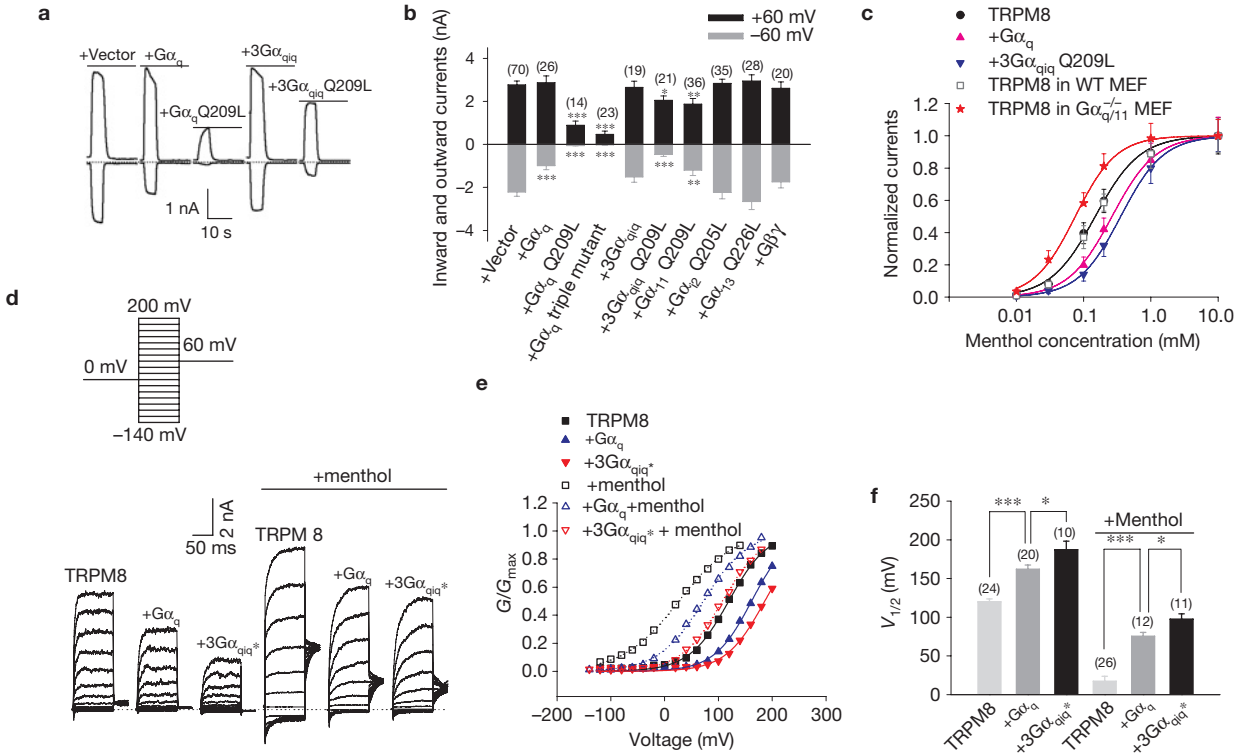

Figure 4 Activated $G\alpha_q$ inhibits TRPM8 independently of the PLC pathway. (**a**) Example of whole-cell inward and outward currents (at −60 mV and +60 mV) activated by menthol (200 μM, 5 s) from HEK293 cells expressing TRPM8 and different $G\alpha_q$ mutants. The dotted line is zero current. (**b**) A summary of the TRPM8-mediated inward and outward currents when transfected with different G-protein subunits in experiments similar to those in **a**. $G\alpha_q$ triple mutant denotes $G\alpha_q$ Q209L/R256A/T257A. The number of experiments is indicated above each bar. (**c**) Normalized whole-cell inward currents at −60 mV as a function of menthol concentration in HEK293 cells or MEF cells expressing TRPM8. Control dose–response curve in HEK293 cells (filled circles), half-maximum effective concentration (EC_{50}) = 148.8 μM (n = 8); co-transfection with $G\alpha_q$ (filled triangles), EC_{50} = 264.4 μM (n = 10); with $3G\alpha_{qiq}$ Q209L (filled downtriangles), EC_{50} = 356.1 μM (n = 9); wild-type MEF cells (open squares), EC_{50} = 156.8 μM (n = 5); $G\alpha_{q/11}^{-/-}$ MEF cells (filled star), EC_{50} = 75.1 μM (n = 7). All curves show the Hill equation with a Hill coefficient of 1.31. (**d**) Representative TRPM8 currents elicited by voltage steps from −140 mV to +200 mV (or to +140 mV in the presence of 100 μM menthol) in 20 mV increments in HEK293 cells expressing TRPM8 and Gα proteins as indicated. The dotted line is zero current. $3G\alpha_{qiq}^*$ denotes the activated Q209L mutant. The voltage-clamp protocol is shown at the top. (**e**) Conductance–voltage relationship for cells in **d** fitted by a Boltzmann function with values of $V_{1/2}$ and steepness factor as follows: TRPM8 alone (filled squares), 119.4 mV, 36.9 mV; $+G\alpha_q$ (filled triangles), 162.4 mV, 35.1 mV; $+3G\alpha_{qiq}^*$ (Q209L, filled downtriangles), 186.1 mV, 36.3 mV; +100 μM menthol (open squares), 26.3 mV, 52.1 mV; $+G\alpha_q$ + menthol (open triangles), 71.7 mV, 41.9 mV; $+3G\alpha_{qiq}^*$ + menthol (open downtriangles), 107.3 mV, 38.8 mV. (**f**) A summary of the $V_{1/2}$ values from experiments similar to those in **d**. The number of experiments is given above each bar. All error bars are mean ± s.e.m. $^*P < 0.05$; $^{**}P < 0.01$; $^{***}P < 0.001$.

presumably caused by a flickering opening of TRPM8 channels (see below Fig. 7a,b). These results show that TRPM8 activation, whether by menthol or by depolarization, is inhibited by active $G\alpha_q$ by shifting the voltage dependence of TRPM8 towards more positive membrane potentials. The strong inhibition caused by the signalling-ablated mutant $3G\alpha_{qiq}$ Q209L shows that inhibition occurs without engagement of downstream signalling pathways.

Inflammatory mediators inhibit TRPM8 through a direct action of activated $G\alpha_q$

To further investigate whether the coupling of the $3G\alpha_{qiq}$ chimaera to PLCβ is completely disabled, we transfected the PIP_2 reporter Tubby–R332H–cYFP along with the BK receptor into $G\alpha_{q/11}$-null MEF cells. Tubby rapidly translocated to the cytoplasm following BK treatment when wild-type $G\alpha_q$ was co-transfected, but there was no translocation with the $3G\alpha_{qiq}$ chimaera (Fig. 5a,b). Similar results were obtained with another PLCβ signalling reporter PLCδ-PH–EGFP (Supplementary Fig. S4b,c). These data indicate that the $3G\alpha_{qiq}$ chimaera lacks the ability to activate PLCβ.

We then used the $3G\alpha_{qiq}$ chimaera in gain-of-function experiments in the $G\alpha_{q/11}$-deficient MEF cells. Histamine caused no suppression of TRPM8 activity, confirming the complete deletion of $G\alpha_{q/11}$ in the MEF cells, but transfection of the $3G\alpha_{qiq}$ chimaera rescued suppression (Fig. 5c,d and Supplementary Fig. S2d). Similarly, the $3G\alpha_{qiq}$ chimera also rescued BK-mediated inhibition of TRPM8 currents (Fig. 5e,f and Supplementary Fig. S2c). The rescue of coupling from GPCRs to TRPM8 by $3G\alpha_{qiq}$, which is unable to couple to PLCβ, confirms that $G\alpha_q$ couples directly to TRPM8 without the need to involve signalling pathways downstream of PLC.

$G\alpha_q$ binds directly to TRPM8

Direct modulation of TRPM8 by $G\alpha_q$ suggests that they might form a complex. Figure 6a shows that both wild-type $G\alpha_q$ and active $G\alpha_q$ Q209L were pulled down by TRPM8 to a similar extent. Reciprocally, TRPM8 was co-precipitated by either $G\alpha_q$ or $G\alpha_q$ Q209L (Fig. 6b). Co-precipitation between TRPM8 and $G\alpha_q$ was also observed in native DRG neurons (Fig. 6c). Both the amino- and carboxy-terminal domains of TRPM8 bind to $G\alpha_q$ and to $G\alpha_q$ Q209L, although stronger

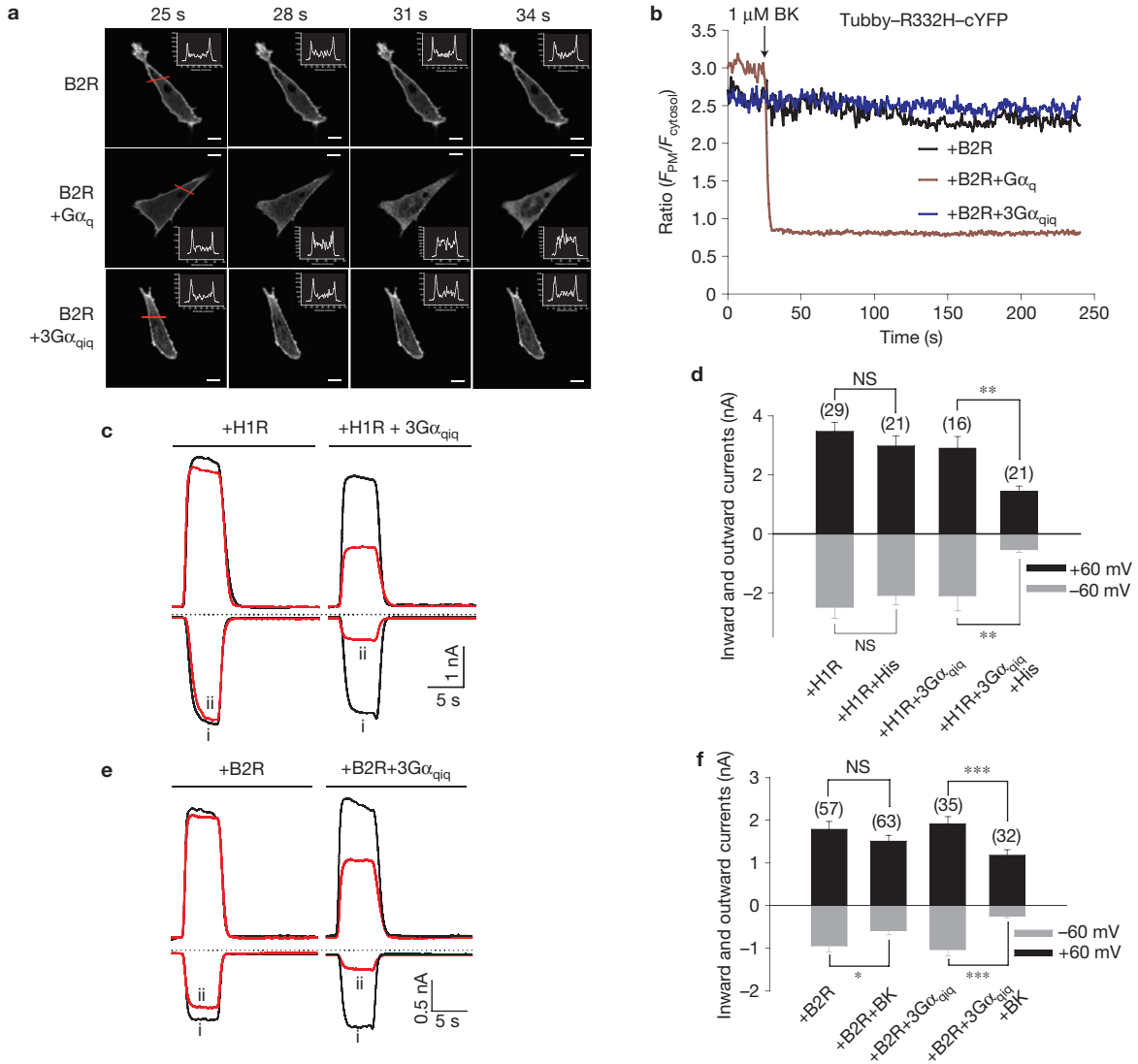

Figure 5 Inflammatory mediators inhibit TRPM8 through a direct action of activated Gαq. (**a**) Translocation of Tubby–R332H–cYFP induced by BK in $G\alpha_{q/11}^{-/-}$ MEF cells co-transfected with B2R and G proteins as indicated. BK (1 μM) was added at 25 s. Scale bar, 10 μm. Profiles of the intensity across cells (indicated by red line) are shown inset at the corner of the images. (**b**) Quantification of relative membrane Tubby fluorescence signal as a function of time in **a**. Each experiment was repeated at least four times with similar results. (**c**) Typical traces of TRPM8 inward and outward currents (at −60 mV and +60 mV), activated by menthol (200 μM, 5 s) in $G\alpha_{q/11}^{-/-}$ MEF cells transfected with H1R and TRPM8. Currents shown before (i) and after (ii) histamine addition (10 μM, 1 min). The dotted line is zero current. (**d**) A summary of results similar to those in **c**. The number of experiments is shown above each bar. All data are mean ± s.e.m. $^{**}P < 0.01$; NS, not significant. (**e**) Similar experiments with application of BK (1 μM) to $G\alpha_{q/11}^{-/-}$ MEF cells expressing B2R. (**f**) A summary of results similar to those in **e**. All error bars are mean ± s.e.m. $^{*}P < 0.05$; $^{***}P < 0.001$; NS, not significant.

binding was observed to the N terminus (Fig. 6d). Neither $G\alpha_{i2}$ nor Gαs showed significant binding to TRPM8 under similar conditions (Supplementary Fig. S5a–c). Furthermore, neither BK nor histamine promoted binding of $G\alpha_q$ to TRPM8 (Fig. 6e). Thus, $G\alpha_q$ and TRPM8 form a constitutive complex, and activation of $G\alpha_q$ by a GPCR does not enhance binding.

We next delineated the functional TRPM8-binding region on $G\alpha_q$ by making a series of chimaeras between active forms of $G\alpha_q$, which binds to and activates TRPM8, and $G\alpha_i$, which does not (shown schematically in Fig. 6f). All chimaeras were similarly expressed, and none affected TRPM8 expression (Supplementary Fig. S5d,e). Chimaeras $G\alpha_{qi}$ and $2G\alpha_{qi}$ activated PIP_2 hydrolysis in a similar manner to $G\alpha_q$ Q209L. However, $3G\alpha_{qi}$ lacked the ability to hydrolyse PIP_2 (Supplementary Fig. S4a), showing that the PLCβ-binding region on $G\alpha_q$ is located between Glu 245 and Tyr 261, in agreement with other findings[26]. Interestingly, this chimaera still inhibited TRPM8 inward and outward currents, but a progressive loss of inhibition was found in chimaeras $4G\alpha_{qi}$ and $5G\alpha_{qi}$ (Fig. 6f), and a corresponding loss of binding to TRPM8 was observed with the same deletions (Supplementary Fig. S5d), indicating that the region between Asn 222 and Glu 245 on $G\alpha_q$ contains the functional TRPM8-binding region required for the modulation of TRPM8. This region corresponds to the Switch III helix region of $G\alpha_q$, which is structurally one of the most mobile regions and has extensive contacts with effectors. A modelled structure of heterotrimeric $G\alpha_q\beta\gamma$ indicates that the Switch III loop protrudes out of the protein surface and is free to be engaged by effectors such as TRPM8 (Supplementary Fig. S6). TRPM8 and PLCβ therefore bind to

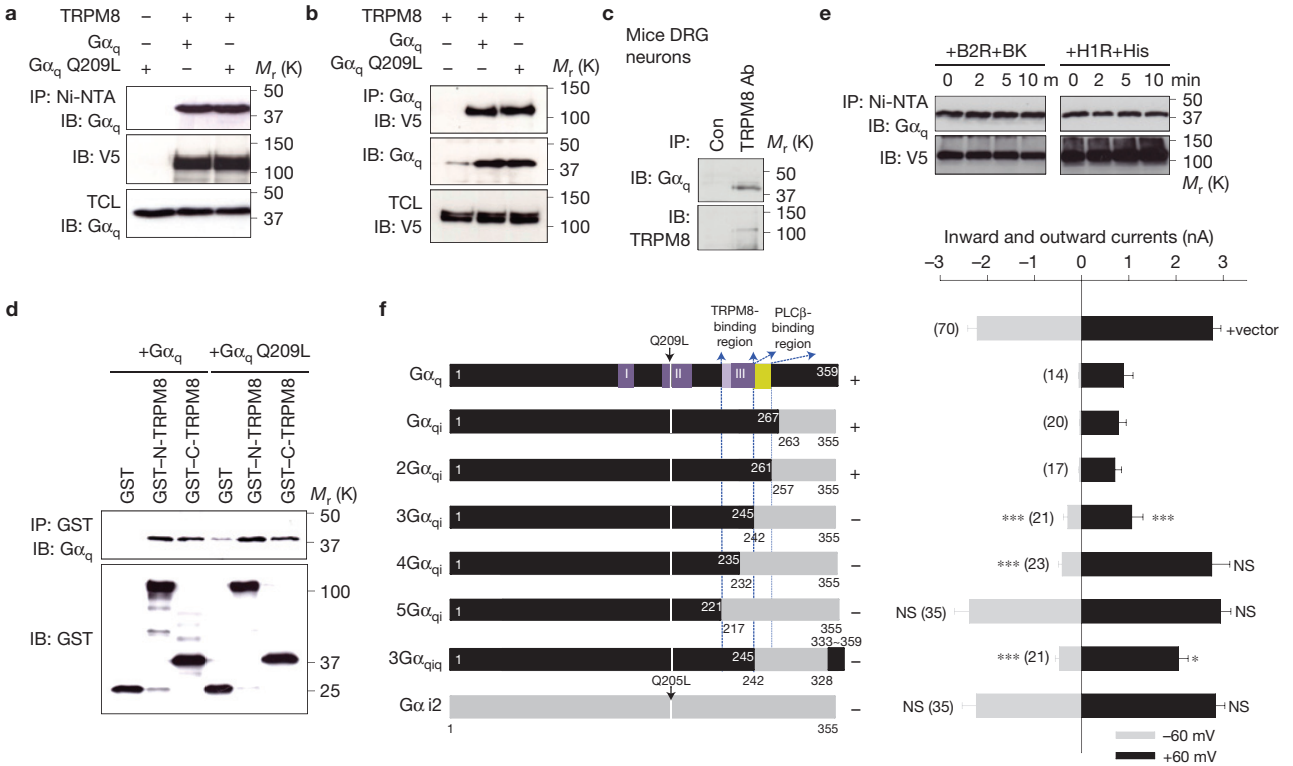

Figure 6 Direct interaction of TRPM8 with $G\alpha_q$. (**a**,**b**) Mutual co-precipitation between TRPM8 and $G\alpha_q$. HEK293 cell lysate expressing TRPM8–V5–hexahistidine and $G\alpha_q$/$G\alpha_q$ Q209L was pulled down by either nickel beads (**a**) or $G\alpha_q$ antibody (**b**), and co-precipitated $G\alpha_q$ (**a**) or TRPM8 (**b**) was detected with the indicated antibodies (top blots). The same blots stripped and reprobed with anti-V5 (**a**) or anti-$G\alpha_q$ (**b**) (middle blots). The bottom blots show similar $G\alpha_q$ (**a**) or TRPM8 (**b**) expression in total cell lysate (TCL) in all cases. IP, immunoprecipitation; IB, immunoblot. (**c**) In DRG neurons $G\alpha_q$ was co-precipitated by TRPM8 (top). The same blot reprobed with anti-TRPM8 (bottom). Specificity is shown by the omission of the TRPM8 antibody from the immunoprecipitation solution (Con, left lane). (**d**) $G\alpha_q$ and $G\alpha_q$ Q209L bind to the TRPM8 N and C termini. GST-coupled TRPM8 N and C termini were used to pull down cell lysate expressing $G\alpha_q$ or $G\alpha_q$ Q209L (top blot). The N terminus binds 1.28 ± 0.025 fold more $G\alpha_q$ than does the C terminus ($n = 3$). Blot stripped and reprobed with anti-GST (bottom). (**e**) BK and histamine did not enhance the binding of $G\alpha_q$ to TRPM8. Cells expressing TRPM8–V5–hexahistidine and B2R or H1R were treated with DSP after exposure to BK (1 μM, left) or histamine (10 μM, right) for different times. TRPM8 was pulled down by Ni-NTA, and the associated $G\alpha_q$ was detected by anti-$G\alpha_q$ (top blot). Blots reprobed with anti-V5 (bottom). (**f**) TRPM8 binds to the switch III region on $G\alpha_q$, resulting in the suppression of TRPM8. On the left is a schematic diagram of the chimaeras between $G\alpha_q$ Q209L (black bars) and $G\alpha_{i2}$ Q205L (grey bars). The number of amino acids in each protein used for the chimaera is given at the top corner of the black bars ($G\alpha_q$ Q209L), or underneath the grey bars ($G\alpha_{i2}$ Q205L). Switch I, II and III regions on $G\alpha_q$ are purple, TRPM8- and PLCβ-binding regions are indicated by dotted blue lines. The ability of chimaeras to activate PLCβ (Supplementary Fig. S4a) is indicated to the right of each chimaera: +, activated; −, ineffective. The second bar from the bottom shows construction of $3G\alpha_{qiq}$ in which the distal C terminus of $G\alpha_q$ (Asp 333–Val 359) has been transplanted back into $3G\alpha_{qi}$ to allow coupling to G_q-coupled GPCRs. Right: A summary of the inhibition of TRPM8 currents caused by the chimaeras shown on the left. The number of experiments is shown to the left of each bar. Error bars, s.e.m. $^*P < 0.05$; $^{***}P < 0.001$; NS, not significant. Uncropped images of blots (**a**–**e**) are shown in Supplementary Fig. S8.

distinct but contiguous regions on $G\alpha_q$, rendering their mutual and independent regulation by $G\alpha_q$ possible.

Activated $G\alpha_q$ directly inhibits TRPM8 in excised patches

If activated $G\alpha_q$ protein inhibits TRPM8 without the intervention of downstream signalling pathways, then the inhibition should be detectable in excised TRPM8-containing patches. TRPM8 channel activity runs down immediately after excision owing to rapid loss of PIP_2 (refs 14,15), but channels then remain active at a constant low level. Subsequent application of a water-soluble dioctanoyl (DiC8)-PIP_2 restored channel activity to an even higher level (Supplementary Fig. S7a). We applied purified $G\alpha_q$ protein, activated by prior incubation with GTP-γS, to the intracellular surface of excised patches when channel run-down was complete and activity had become stable. Activated $G\alpha_q$ rapidly reduced the TRPM8 open probability (Supplementary Fig. S7b), an effect that could be due to activation of residual PLCβ trapped in the patch, and a consequent further reduction in levels of PIP_2. We found, however, that the inhibition of TRPM8 by activated $G\alpha_q$ was even more prominent in the presence of saturating levels of DiC8-PIP_2, which strongly activates TRPM8 (Fig. 7a,b). In control experiments, application of $G\alpha_q$ incubated with GDP-βS (which forces $G\alpha_q$ into the inactive state), boiled $G\alpha_q$, Gβγ or the activation buffer without either GTP-γS or $G\alpha_q$, were all without effect (Fig. 7e).

We showed above that $G\alpha_q$ constitutively binds to TRPM8. Endogenous $G\alpha_q$ should therefore remain in excised patches, associated with TRPM8, and should inhibit TRPM8 when switched into an active state. Consistent with this idea, addition of non-hydrolysable GTP-γS, but not GDP-βS, to inside-out membrane patches reduced the TRPM8 open probability both in the presence or absence of exogenous DiC8-PIP2 (Fig. 7c–e and Supplementary Fig. S7c). In experiments on patches excised from MEF cells lacking endogenous $G\alpha_{q/11}$ the application of activated $G\alpha_q$ itself inhibited TRPM8 as in patches from HEK293 cells, but the inhibitory effect of GTP-γS alone was absent (Fig. 7e), confirming that $G\alpha_q$ remaining in the patch is indeed responsible for

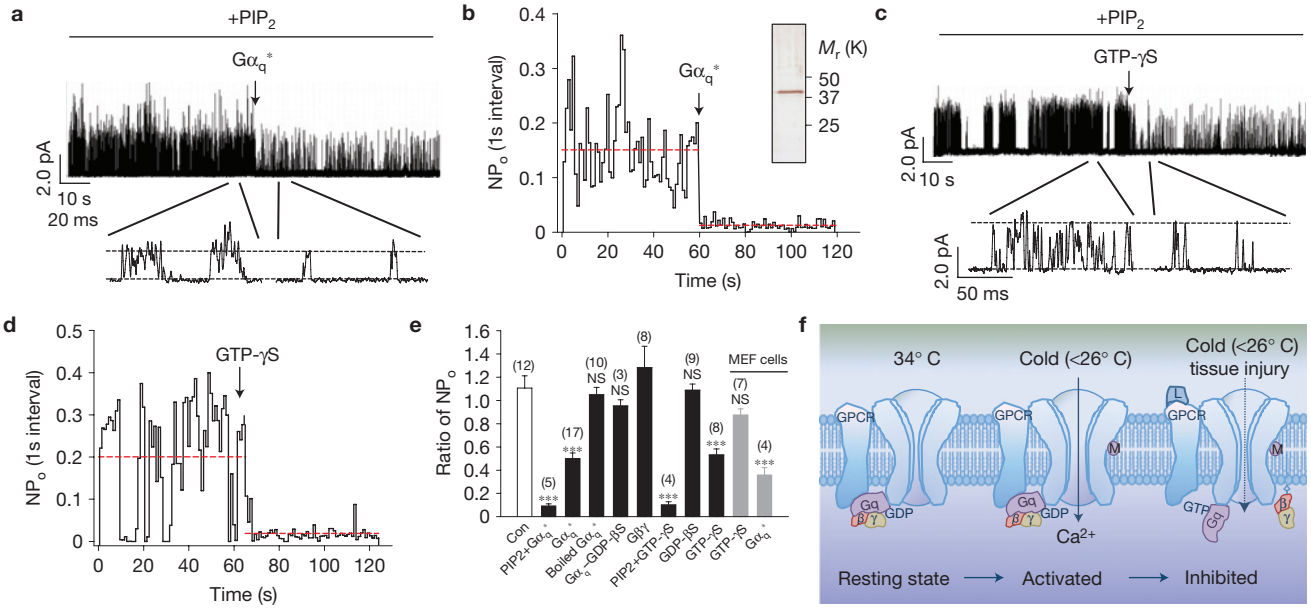

Figure 7 Activated $G\alpha_q$ directly inhibits TRPM8 in excised patches. (**a**) Left: A typical example of the channel activity at +40 mV in inside-out patches excised from HEK293 cells expressing TRPM8 after the addition of 50 nM $G\alpha_q^*$ ($G\alpha_q$ pre-incubated with GTP-γS) in the presence of 50 μM DiC8-PIP_2. The arrow indicates the time of addition of $G\alpha_q^*$. Sections of traces are shown below at a higher time resolution. Note that single-channel currents are smaller than in Fig. 3a, because the membrane potential was lower. (**b**) Real-time quantification of NP_o in **a**. The red dashed lines give the mean NP_o over the indicated time period. The inset shows silver staining of purified $G\alpha_q$ protein. Mean NP_o before $G\alpha_q^*$ addition, 0.151 ± 0.0088; after $G\alpha_q^*$ addition, 0.013 ± 0.001; $P < 0.001$. (**c**) A similar experiment to **a**, but with the application of 100 μM GTP-γS. (**d**) Real-time quantification of NP_o in **c**. The red dashed lines give the mean NP_o over the indicated time period. NP_o before GTP-γS addition, 0.20 ± 0.016; after GTP-γS addition, 0.019 ± 0.0027; $P < 0.001$. (**e**) Mean values of ratios of NP_o for treatments shown below bars (the ratio is the mean value over the period 1 min after application, to that 1 min before; see plots in **b**,**d**). The number of experiments is given above each bar. All data are mean ± s.e.m. $^{***}P < 0.001$ compared with control solution; NS, not significant relative to control. (**f**) Schematic depicting the proposed mechanism for the regulation of TRPM8 by the $G\alpha_q$ subunit. Left: In the resting state at 34 °C, TRPM8 is pre-bound to $G\alpha_q$. The TRPM8 activity is low at this temperature. Middle: Cold temperature or a cooling compound such as menthol (M) activates TRPM8, resulting in an inward current flow and an increase in the firing frequency of cold fibres. Right: Inflammatory mediators (L) released by tissue injury bind to a GPCR resulting in GTP–GDP exchange and consequent activation of $G\alpha_q$. The consequent conformational change in $G\alpha_q$ causes inhibition of TRPM8 by a direct interaction, resulting in a decrease in current passing into the nerve terminal through TRPM8 and so a decreased firing of cold-sensitive nerve fibres.

TRPM8 inhibition. This experiment also shows that subunits other than $G\alpha_{q/11}$ are not able to inhibit TRPM8 following activation by GTP-γS.

DISCUSSION

Three mechanisms for the modulation of ion channels by GPCRs have been well established. Channels can be modulated through phosphorylation by kinases such as PKA, PKC or Src (refs 28,29), by direct binding to Gβγ subunits released following GPCR activation[30,31] or by interaction with membrane PIP_2 (refs 32–35). We provide here evidence for a fourth mechanism: the $G\alpha_q$ subunit binds directly to TRPM8, and the conformational change of $G\alpha_q$ following GPCR activation causes a rapid and direct *trans*-inhibition of TRPM8 (Fig. 7f). It is tempting to speculate that the $G\alpha_q$ subunit could be involved in the regulation of other ion channels, a possibility that can now be investigated by the use of our $3G\alpha_{qiq}$ chimaera, which allows unequivocal discrimination of a direct action of activated $G\alpha_q$ from downstream actions triggered by the PLC signalling pathway.

Previous studies have demonstrated that PIP_2 is a potent activator of TRPM8 (refs 14–16). A decrease in membrane PIP_2 following activation of a Gq-coupled GPCR could therefore be responsible for inhibiting TRPM8. In the present study we confirmed that activation of Gq-coupled GPCRs caused a marked PIP_2 depletion. Unexpectedly, our evidence argues against a major physiological role for PIP_2 depletion in TRPM8 inhibition, because inhibiting PLC had little effect on TRPM8 inhibition following activation of Gq-coupled GPCRs, whereas a $G\alpha_q$ construct completely decoupled from PLC still had a strong action. Therefore, direct inhibition by activated $G\alpha_q$ is the main cause of the inhibition. A likely explanation for the lack of involvement of PIP_2 is that following activation of a G_q-coupled GPCR, TRPM8 is rapidly engaged and inhibited by activated $G\alpha_q$ even before the downstream PLCβ signalling pathway is initiated, so that subsequent PIP_2 depletion cannot further inhibit the channels. Another possibility is that the binding affinity of TRPM8 channels for PIP_2 is high, so that channels remain fully occupied by PIP_2 even when PIP_2 has been depleted by activation of PLC (refs 32,35).

We found that $G\alpha_q$ binds to TRPM8 even when inactive, and that binding was not enhanced by activation of $G\alpha_q$. It is likely that inactive $G\alpha_q$ binds to TRPM8 at an interface that differs from that of activated $G\alpha_q$, and that a conformational change on activation causes a reorientation of $G\alpha_q$ to interact with a different site on TRPM8 (Fig. 7). We base this proposal on the observation that in isolated membrane patches, application of activated $G\alpha_q$ is able to inhibit TRPM8, even though TRPM8 is already bound to endogenous inactive $G\alpha_q$. $G\alpha_q$ thus functions as an integral component of the TRPM8 gating machinery, controlling the opening of TRPM8 channels and allowing rapid and efficient signal transduction. A similar association is also observed between $G\alpha_q$ and PLCβ, which form a preassembled complex[36], and in which activation of $G\alpha_q$ does not increase the association with PLCβ (ref. 37).

A recent study has also reported an interaction between TRPM8 and $G\alpha_q$ (ref. 38). This study showed that activation of TRPM8 causes downstream activation of the $G\alpha_q$–PLC metabotropic pathway. This effect is in the opposite direction to the $G\alpha_q$-to-TRPM8 inhibition demonstrated in the present paper, and raises the possibility that not only can $G\alpha_q$ influence the gating of TRPM8, as shown here, but that the gating of TRPM8 may also influence $G\alpha_q$. Activation of TRPM8 could in this scenario activate $G\alpha_q$, which would then inhibit TRPM8. In the absence of external Ca^{2+}, however, there is little rebound inhibition of TRPM8 currents following activation by menthol (see, for example, Fig. 4a), suggesting that any activation of $G\alpha_q$ by TRPM8 plays only a minor role in the gating of TRPM8.

The sensory information provided by cold-sensitive nerve terminals expressing TRPM8 is involved in the conscious sensation of coolness, in the detection of skin-surface dryness and in cold allodynia[11,19]. The evidence that inflammatory mediators can inhibit the activity of cold-sensitive nerve terminals by a direct action of $G\alpha_q$ on TRPM8 has relevance for the understanding of cold dysesthesias associated with injury and inflammation. Elucidating the molecular mechanism involved in the modulation of cold-evoked activity under inflammatory conditions opens up new possibilities for its selective therapeutic manipulation. □

METHODS

Methods and any associated references are available in the online version of the paper.

Note: Supplementary Information is available in the online version of the paper

ACKNOWLEDGEMENTS

We thank S. Offermanns (Max Planck Institute for Heart and Lung Research, Germany) for providing MEF cells, G. Hammond (Department of Pharmacology, University of Cambridge, UK) for Tubby–R332H–cYFP and PLCδ-PH–EGFP cDNA and for help with imaging analysis, O. Opaleye (Department of Biochemistry, University of Cambridge, UK) for help with protein purification, R. Hardie (Department of Physiology, Development and Neuroscience, University of Cambridge, UK) and S.B. Hladky (Department of Pharmacology, University of Cambridge, UK) for help with single-channel recording, and R. Hardie for critical reading of an earlier version of the manuscript. This work was supported by an MRC new investigator research grant (G0801387 to X.Z.), a BBSRC research grant (BB/F003072/1 to P.A.M.) and a grant from the Fundacion BBVA (to P.A.M., to support a BBVA visiting professorship at the Instituto de Neurociencias, Alicante, Spain).

AUTHOR CONTRIBUTIONS

X.Z. came up with the hypothesis, designed and performed experiments, and analysed data except calcium imaging experiments, which were carried out by S.M., and nerve fibre recordings, which were carried out by A.P, B.D., C.B. and P.A.M.; L.L. assisted with molecular biology experiments and neuron preparation. X.Z. wrote the manuscript with input from C.B. and P.A.M. X.Z. and P.A.M. supervised the project.

COMPETING FINANCIAL INTERESTS

The authors declare no competing financial interests.

Published online at www.nature.com/doifinder/10.1038/ncb2529
Reprints and permissions information is available online at www.nature.com/reprints

1. Cesare, P. & McNaughton, P. A novel heat-activated current in nociceptive neurons and its sensitization by bradykinin. *Proc. Natl Acad. Sci. USA* **93,** 15435–15439 (1996).
2. Numazaki, M., Tominaga, T., Toyooka, H. & Tominaga, M. Direct phosphorylation of capsaicin receptor VR1 by protein kinase Cepsilon and identification of two target serine residues. *J. Biol. Chem.* **277,** 13375–13378 (2002).
3. Bhave, G. *et al.* Protein kinase C phosphorylation sensitizes but does not activate the capsaicin receptor transient receptor potential vanilloid 1 (TRPV1). *Proc. Natl Acad. Sci. USA* **100,** 12480–12485 (2003).
4. Zhang, X., Huang, J. & McNaughton, P. A. NGF rapidly increases membrane expression of TRPV1 heat-gated ion channels. *EMBO J.* **24,** 4211–4223 (2005).
5. Zhang, X., Li, L. & McNaughton, P. A. Proinflammatory mediators modulate the heat-activated ion channel TRPV1 via the scaffolding protein AKAP79/150. *Neuron* **59,** 450–461 (2008).
6. Peier, A. M. *et al.* A TRP channel that senses cold stimuli and menthol. *Cell* **108,** 705–715 (2002).
7. McKemy, D. D., Neuhausser, W. M. & Julius, D. Identification of a cold receptor reveals a general role for TRP channels in thermosensation. *Nature* **416,** 52–58 (2002).
8. Proudfoot, C. J. *et al.* Analgesia mediated by the TRPM8 cold receptor in chronic neuropathic pain. *Curr. Biol.* **16,** 1591–1605 (2006).
9. Dhaka, A. *et al.* TRPM8 is required for cold sensation in mice. *Neuron* **54,** 371–378 (2007).
10. Colburn, R. W. *et al.* Attenuated cold sensitivity in TRPM8 null mice. *Neuron* **54,** 379–386 (2007).
11. Chung, M. K. & Caterina, M. J. TRP channel knockout mice lose their cool. *Neuron* **54,** 345–347 (2007).
12. Daniels, R. L. & McKemy, D. D. Mice left out in the cold: commentary on the phenotype of TRPM8-nulls. *Mol. Pain* **3,** 23–26 (2007).
13. Xing, H., Chen, M., Ling, J., Tan, W. & Gu, J. G. TRPM8 mechanism of cold allodynia after chronic nerve injury. *J. Neurosci.* **27,** 13680–13690 (2007).
14. Rohacs, T., Lopes, C. M., Michailidis, I. & Logothetis, D. E. PI(4, 5)P2 regulates the activation and desensitization of TRPM8 channels through the TRP domain. *Nat. Neurosci.* **8,** 626–634 (2005).
15. Liu, B. & Qin, F. Functional control of cold- and menthol-sensitive TRPM8 ion channels by phosphatidylinositol 4,5-bisphosphate. *J. Neurosci.* **25,** 1674–1681 (2005).
16. Varnai, P., Thyagarajan, B., Rohacs, T. & Balla, T. Rapidly inducible changes in phosphatidylinositol 4,5-bisphosphate levels influence multiple regulatory functions of the lipid in intact living cells. *J. Cell Biol.* **175,** 377–382 (2006).
17. Premkumar, L. S., Raisinghani, M., Pingle, S. C., Long, C. & Pimentel, F. Downregulation of transient receptor potential melastatin 8 by protein kinase C-mediated dephosphorylation. *J Neurosci.* **25,** 11322–11329 (2005).
18. Linte, R. M., Ciobanu, C., Reid, G. & Babes, A. Desensitization of cold- and menthol-sensitive rat dorsal root ganglion neurones by inflammatory mediators. *Exp. Brain Res.* **178,** 89–98 (2007).
19. Parra, A. *et al.* Ocular surface wetness is regulated by TRPM8-dependent cold thermoreceptors of the cornea. *Nat. Med.* **16,** 1396–1399 (2010).
20. Cesare, P., Dekker, L. V., Sardini, A., Parker, P. J. & McNaughton, P. A. Specific involvement of PKC-epsilon in sensitization of the neuronal response to painful heat. *Neuron* **23,** 617–624 (1999).
21. Koike-Tani, M. *et al.* Signal transduction pathway for the substance P-induced inhibition of rat Kir3 (GIRK) channel. *J. Physiol.* **564,** 489–500 (2005).
22. Chen, X. *et al.* Inhibition of a background potassium channel by Gq protein α-subunits. *Proc. Natl Acad. Sci. USA* **103,** 3422–3427 (2006).
23. Wu, D. Q., Lee, C. H., Rhee, S. G. & Simon, M. I. Activation of phospholipase C by the α subunits of the Gq and G11 proteins in transfected Cos-7 cells. *J. Biol. Chem.* **267,** 1811–1817 (1992).
24. Takasaki, J. *et al.* A novel Gαq/11-selective inhibitor. *J. Biol. Chem.* **279,** 47438–47445 (2004).
25. Quinn, K. V., Behe, P. & Tinker, A. Monitoring changes in membrane phosphatidylinositol 4,5-bisphosphate in living cells using a domain from the transcription factor tubby. *J. Physiol.* **586,** 2855–2871 (2008).
26. Venkatakrishnan, G. & Exton, J. H. Identification of determinants in the α-subunit of Gq required for phospholipase C activation. *J. Biol. Chem.* **271,** 5066–5072 (1996).
27. Offermanns, S. *et al.* Embryonic cardiomyocyte hypoplasia and craniofacial defects in Gαq/Gα11-mutant mice. *EMBO J.* **17,** 4304–4312 (1998).
28. Yao, X., Kwan, H. Y. & Huang, Y. Regulation of TRP channels by phosphorylation. *Neurosignals* **14,** 273–280 (2005).
29. Huang, J., Zhang, X. & McNaughton, P. A. Modulation of temperature-sensitive TRP channels. *Semin. Cell Dev. Biol.* **17,** 638–645 (2006).
30. Clapham, D. E. & Neer, E. J. G protein βγ subunits. *Annu. Rev. Pharmacol. Toxicol.* **37,** 167–203 (1997).
31. Dascal, N. Ion-channel regulation by G proteins. *Trends Endocrinol. Metab* **12,** 391–398 (2001).
32. Gamper, N. & Shapiro, M. S. Regulation of ion transport proteins by membrane phosphoinositides. *Nat. Rev. Neurosci.* **8,** 921–934 (2007).
33. Brown, D. A., Hughes, S. A., Marsh, S. J. & Tinker, A. Regulation of M(Kv7.2/7.3) channels in neurons by PIP(2) and products of PIP(2) hydrolysis: significance for receptor-mediated inhibition. *J. Physiol.* **582,** 917–925 (2007).
34. Nilius, B., Owsianik, G. & Voets, T. Transient receptor potential channels meet phosphoinositides. *EMBO J.* **27,** 2809–2816 (2008).
35. Suh, B. C. & Hille, B. PIP2 is a necessary cofactor for ion channel function: how and why? *Annu. Rev. Biophys.* **37,** 175–195 (2008).
36. Dowal, L., Provitera, P. & Scarlata, S. Stable association between Gα(q) and phospholipase Cβ1 in living cells. *J. Biol. Chem.* **281,** 23999–24014 (2006).
37. Grubb, D. R., Vasilevski, O., Huynh, H. & Woodcock, E. A. The extreme C-terminal region of phospholipase Cβ1 determines subcellular localization and function; the 'b' splice variant mediates α1-adrenergic receptor responses in cardiomyocytes. *FASEB J.* **22,** 2768–2774 (2008).
38. Klasen, K. *et al.* The TRPM8 ion channel comprises direct Gq protein-activating capacity. *Pflugers Arch.* **463,** 779–797 (2012).

METHODS

Single-unit recordings. Corneal nerve fibre recording was performed as described previously[19]. Briefly, eyes of adult C57BL/6J mice were removed and placed in a recording chamber perfused with the saline solution. A fire-polished glass recording pipette filled with physiological saline was applied to the surface of the corneal epithelium with slight suction to make extracellular recordings of nerve activity. Signals were amplified with an a.c. amplifier and data were captured and analysed using a CED 1401 interface coupled to a computer running Spike26.0 software.

Tongue nerve fibre recording was performed in isolated tongues from adult male C57BL/6J mice. The tongue was removed from the head and the right and left lingual nerves were isolated. The tongue was then transferred to a recording chamber continuously perfused with saline solution at 35 °C. The distal end of one of the lingual nerves was placed in an adjoining compartment filled with paraffin oil and split into smaller filaments. A filament was placed on a monopolar platinum wire electrode connected to an amplifier to record impulse activity. When a filament exhibiting spontaneous activity was detected, a cold ramp down to around 10 °C was delivered. Nerve filaments showing multi-unit background discharge with cooling were further divided until a nerve filament containing a single or a few active units was obtained. To induce an acute inflammation in the tongue, animals were injected with lambda carrageenan (2% in saline, 5 µl) down the midline towards the tip of the underside of the tongue. This caused a marked tissue edema that was fully developed two hours later. The mouse was then euthanized and the tongue was prepared and recorded in the same manner as above.

Cell culture and transfection. HEK293 cells and MEF cells were maintained in DMEM medium containing 10% fetal bovine serum, 100 UI ml^{-1} penicillin, 100 µg ml^{-1} streptomycin and 2.0 mM L-glutamine. For electrophysiology, HEK293 cells were transiently transfected using PolyFect transfection reagents (QIAGEN) according to the manufacturer's instructions. MEF cells were transfected by using cell line nucleofection kits (Lonza). Electrophysiology recordings were typically performed 2–3 days following transfection. For molecular biology experiments, we use TurboFect transfection reagent (Fermentas).

DRG neuron isolation and culture were conducted as described previously[4,5].

Molecular biology. Human $G\alpha_{q/11}$, $G\alpha_{i2}$, $G\beta_1$, $G\gamma_2$, $G\alpha_s$, $G\alpha_{13}$ and H1R receptor complementary DNAs were purchased from Missouri S&T cDNA Resource Center. GST-coupled TRPM8 N- and C- terminal fragments and all $G\alpha_q$ chimaeras were constructed by standard PCR procedures. TRPM8 tagged with V5 and hexahistidine epitopes at the C terminus were as described previously[5]. Mutagenesis was performed by using a QuikChange site-directed mutagenesis kit (Stratagene).

To pull down hexahistidine-tagged TRPM8 with nickel beads, HEK293 cells transfected with TRPM8–V5–His and $G\alpha_q$ were solubilized in a lysis buffer consisting of 20 mM HEPES, 1.0% NP40, 150 mM NaCl, 0.4 mM EDTA and 20 mM imidazole plus protease inhibitor cocktail (Roche). Ni-NTA agarose beads (QIAGEN) were then incubated with cell lysate at 4 °C followed by extensive washing with the lysis buffer. For GST pulldown, approximately 0.2 µg of purified GST-coupled N- (1–691) and C-terminal (980–1,104) protein fragments from BL-21 cells were incubated with either purified $G\alpha_q$ protein or cell lysate overexpressing $G\alpha_q$/$G\alpha_q$ Q209L at 4 °C for 3 h, followed by overnight incubation with GST–agarose and centrifugation. For crosslinking experiments in Fig. 6e, treated HEK293 cells were incubated with 2.0 mM cell-permeable dithiobis[succinimidyl propionate] (DSP; Pierce) crosslinker for 30 min before solubilization and co-immunoprecipitation. All washed beads were boiled in sample buffer and loaded on 10% SDS–PAGE gel for western blot analysis. Co-immunoprecipitation was performed as described previously[4,5]. For co-immunoprecipitation from DRG neurons in Fig. 6c, TRPM8 antibody (Transgenic, KM060, 1:100) was used to precipitate TRPM8 in DRG neurons, and associated $G\alpha_q$ was detected by monoclonal anti-$G\alpha_q$ (Santa Cruz, sc-136181, 1:1,000). Polyclonal anti-$G\alpha_q$ antibody (Santa Cruz, sc-393, 1: 2,000) that recognizes the $G\alpha_q$ N-terminal domain was used for the detection of $G\alpha_q$ and all chimaeric $G\alpha_q$ proteins. Antibodies against $G\alpha_{i2}$ (sc-13534, 1:2,000) and Gαs (sc-46975, 1:2,000) were from Santa Cruz. All blots were repeated at least three times with similar results.

Electrophysiology. Electrophysiological experiments were performed in calcium-free bath solution unless otherwise stated to prevent desensitization of TRPM8.

Whole-cell patch recording was performed largely as described previously[5]. Briefly, patch electrodes were pulled from thin-walled glass capillaries, and had a resistance of 3.0–4.0 MΩ when filled with internal solution with the following composition: 140 mM KCl, 2.0 mM $MgCl_2$, 5.0 mM EGTA and 10 mM HEPES, adjusted to pH 7.4 with KOH. Cells were perfused with calcium-free bath solution containing: 140 mM NaCl, 4 mM KCl, 10 mM HEPES, 1 mM $MgCl_2$, 5 mM EGTA and 5 mM glucose, adjusted to pH 7.4 with NaOH. For experiments using calcium-containing bath solution, EGTA was replaced with 1.8 mM $CaCl_2$. TRPM8 inward and outward currents were measured at a holding potential of −60 mV and +60 mV, respectively. Cells were pre-treated with 1 µM BK or 10 µM histamine for 1 min before break-in to the whole-cell mode to measure TRPM8 currents activated by menthol. To examine TRPM8 activation by depolarization, steps of voltage pulses were applied for 100 ms ranging from −140 mV to +200 mV in 20 mV increments, followed by a final step to +60 mV. The half-maximal activation voltage ($V_{1/2}$) was obtained as described previously[5] by fitting the normalized channel conductance (G/G_{max})–voltage relationship to a Boltzmann equation: $G/G_{max} = 1/(1+\exp[-(Vm - V_{1/2})/k])$. All recordings were made at room temperature (24 °C) with an Axopatch 200B patch clamp amplifier (Axon) in conjunction with pClampex 10.2 version software (Molecular Devices). Signals were analogue filtered using a 1 kHz low-pass Bessel filter.

Cell-attached and inside-out recordings were made using pipettes fabricated from thick-walled borosilicate glass tubing (Sutter Instrument) with a resistance of 9–15 MΩ when filled with pipette solution. Pipettes were fire polished using a microforge and coated with Sigmacote (Sigma). For inside-out recordings we used a pipette solution with the following composition: 140 mM NaCl, 3 mM KCl and 10 mM HEPES, adjusted to pH 7.3 with NaOH. Bath solution contained: 140 mM KCl, 5 mM EGTA, 1 mM $MgCl_2$, 10 mM HEPES and 5 mM glucose, adjusted to pH 7.3 with KOH. Menthol (500 µM) was included in the pipette solution to activate TRPM8 channels within the patch. Recordings were sampled at 5 kHz and filtered at 2.0 kHz. For the experiments in Fig. 7a,b, 50 µM DiC8-PIP_2 (Echelon Biosciences) was present in the bath solution to prevent TRPM8 channel run-down. Activated G proteins were pulsed onto the excised patches through an ejection pipette positioned close to the patches. Ejection pipettes were connected to a PicoSpritzer III ejection system using nitrogen as a pressure source. Single-channel data were analysed using Clampfit10.2 software (Molecular Devices). Overall channel activities of patches (NP_o) were obtained by using the 50% threshold criterion from the idealized traces[39]. All events were carefully checked visually before being accepted. For representation purposes traces were filtered at 500 Hz.

G-protein purification and activation. $G\alpha_q$ protein was expressed and purified as described previously[40]. Briefly, human $G\alpha_q$, $G\beta_1$ and hexahistidine-tagged $G\gamma_2$ were subcloned into transfer vector PVL1392. Each was co-transfected into Sf9 cells together with baculovirus flashback GOLD expression vector, and recombinant baculoviruses containing G-protein subunits were amplified. Sf9 cells were then infected with a combination of those baculoviruses at a multiplicity of infection of 3.0. Cells were collected 48 h after infection and solubilized by 1% sodium cholate. Proteins were purified using a Ni-NTA agarose column followed by extensive washing. The $G\alpha_q$ subunit was eluted from the column by 30 µM $AlCl_3$ and subsequently purified using a HiTrap Q HP anion exchange column (GE Healthcare). Proteins were eluted with a gradient of NaCl, and peak fractions were collected and assayed by immunoblotting with anti-$G\alpha_q$ antibody. Fractions containing the $G\alpha_q$ protein were pooled and concentrated to 0.3 mg ml^{-1} using an Amicon Ultra filter and stored in aliquots of 3.0 µl at −80 °C.

$G\alpha_q$ protein aliquots were activated in the presence of 0.2 mM dithiothreitol, 1 mM GTP-γS and 0.01% CHAPS in the patch bath solution at 30 °C for 50 min. To remove excess GTP-γS after activation of $G\alpha_q$, the buffer for activated $G\alpha_q$ protein was exchanged by repeated dilution with bath solution and centrifugation by using an AmiconUltra filter. Similar procedures were followed for deactivating $G\alpha_q$ with GDP-βS.

We also purchased purified human $G\alpha_q$ protein from Origene; both sources of purified $G\alpha_q$ protein showed a similar effect. Purified bovine brain Gβγ subunits were obtained from Merck Biosciences.

Fluorescence imaging. Calcium imaging was performed at room temperature as described previously[4]. Briefly, transfected HEK293 cells or DRG neurons were plated onto a coverslip and loaded with Fluo-4-AM (Invitrogen). Cells were continuously perfused with normal Hanks solution and images were collected every 3 s using a Bio-Rad confocal microscope. Pulses of menthol (100 µM) were applied for 15 s every 4 min. BK (1 µM) was applied for 2 min between the fifth and sixth menthol response. The effect of BK was quantified as a response ratio by dividing the sixth by the fifth peak response amplitude. In control experiments on cells not exposed to BK the distribution of response ratios was found to be well fitted by a normal distribution (Supplementary Fig. S1d), from which a threshold ratio was derived at the 95% confidence level and used to determine cells that are significantly inhibited by BK.

DOI: 10.1038/ncb2529

Tubby–R332H–cYFP and PLCδ-PH–EGFP translocation was determined by live scanning using a Leica confocal microscope. Images of MEF cells transfected with the fluorescence probe, B2R and G proteins as appropriate were collected every 0.75 s. Probe translocation was quantified by calculating the ratio of membrane fluorescence to that of cytosol using ImageJ software.

Statistics. All data are mean ± s.e.m. Differences between groups were assessed by either paired (Figs 1a and 3a,b) or unpaired Student's *t*-tests (Fig. 5d,f and Supplementary Fig. S3b), or by one-way analysis of variance with Bonferroni's *post hoc* test (for all other figures). Results were considered significant at $P < 0.05$.

39. Studer, M. & McNaughton, P. A. Modulation of single-channel properties of TRPV1 by phosphorylation. *J. Physiol.* **588,** 3743–3756 (2010).
40. Kozasa, T. & Gilman, A. G. Purification of recombinant G proteins from Sf9 cells by hexahistidine tagging of associated subunits. Characterization of α12 and inhibition of adenylyl cyclase by αz. *J. Biol. Chem.* **270,** 1734–1741 (1995).

DOI: 10.1038/ncb2529

nature cell biology

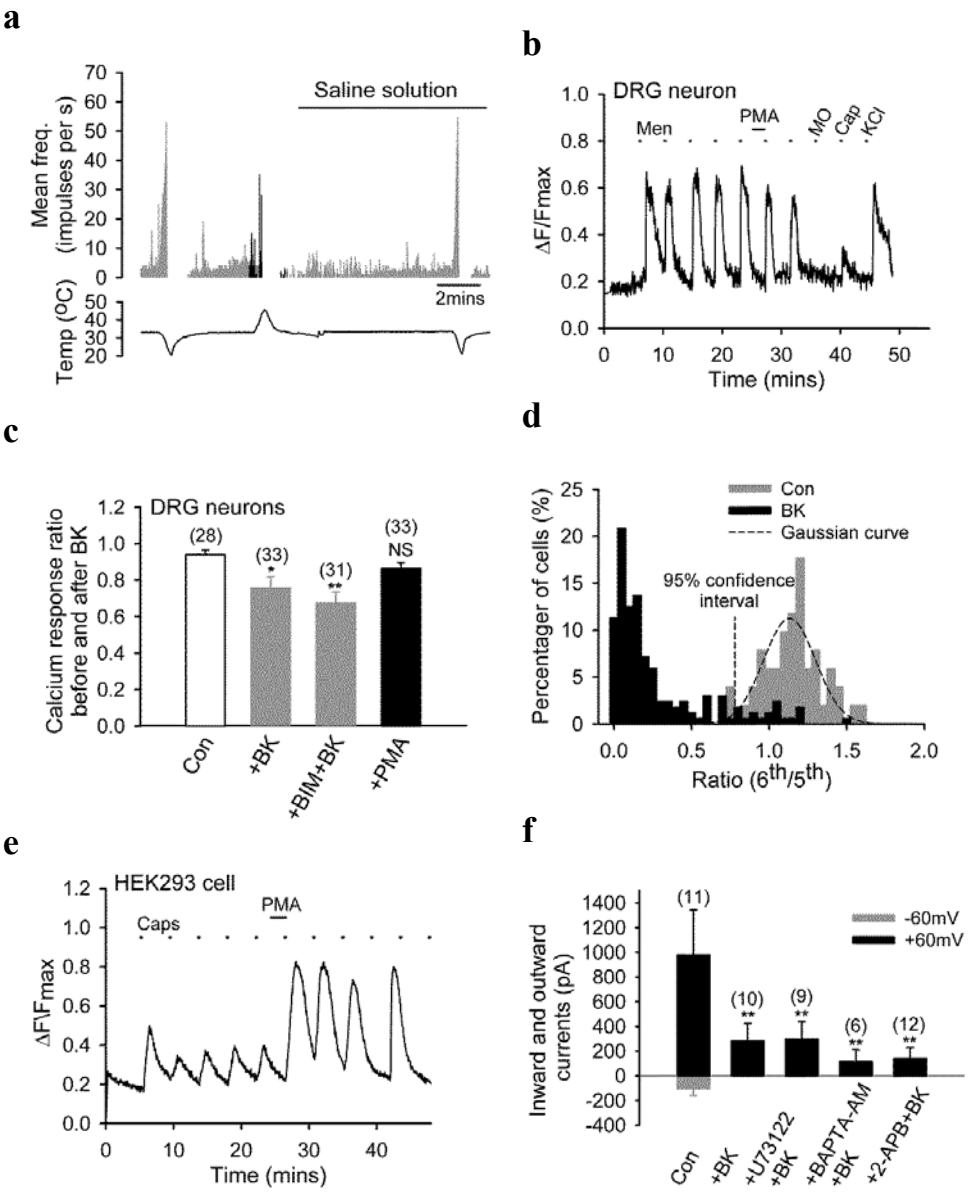

Figure S1 Inhibition of TRPM8 by activation of $G\alpha_q$-coupled GPCRs is independent of downstream signalling pathways. **(a)** Corneal nerve terminal firing frequency in response to cold ramps did not desensitize with successive applications (grey bars) nor following a heat ramp (black bars). Bath temperature shown below. **(b)** In a DRG neuron TRPM8 mediated calcium response activated by menthol (Men, 100mM) were little inhibited when PKC was activated with PMA compared to the effect of BK (see Fig. 2a). 1mM PMA applied for 2 minutes between 5th and 6th menthol-induced response. Calcium increases monitored with Ca-sensitive dye fluo-4. Mustard oil (MO, 50mM), capsaicin (Cap, 100nM), KCl (140mM) applied as shown. **(c)** Summary of mean ratio of peak calcium responses before and after BK treatment in all TRPM8 positive DRG neurons (i.e. those responding and not responding to BK application) from the same experiments as those shown in Fig. 2b. Inhibition by PMA was not significant (final bar). Number of neurons given above each bar. *P<0.05; **P<0.01. **(d)** Distribution of TRPM8-dependent calcium response ratios before (5th response) and after BK (6th response) in HEK293 cells transfected with TRPM8 and B2R, from experiments similar to those in Fig. 2c. Threshold ratio (dashed vertical line) derived from 95% confidence interval of control group was used to determine cells inhibited by BK (85.9% cells inhibited by BK; n_{cell}=61 for control, n_{cell}=168 for BK treated). **(e)** PMA (1mM) caused sensitization of TRPV1 response in a HEK293 cell expressing TRPV1. Capsaicin (Caps, 100nM) applied as indicated. Increase 4.23±0.58-fold (n=15). **(f)** Summary of inhibition of TRPM8 inward and outward currents (at -60mV and +60mV) by BK in similar experiments to those in Fig. 2e, f, but performed with Ca^{2+} containing bath solution, and without EGTA in pipette solution. Cells pre-treated with U73122 (2.5mM, 5mins, bar 3), BAPTA-AM (25mM, 20 mins, bar 4), or 2-aminoethoxydiphenyl borate (2-APB, 100mM, 5 mins, last bar) followed by BK (1mM, 1min). Number of experiments shown above each bar. **P<0.01. All data are mean ± SEM.

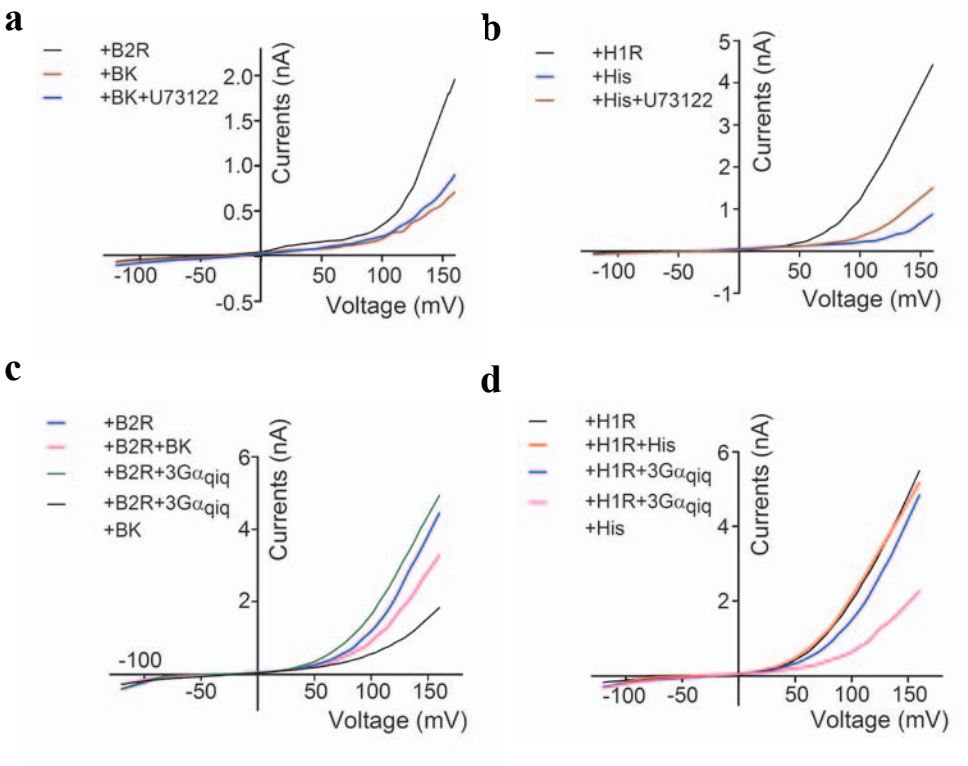

Figure S2 Inhibition of current-voltage relationship of TRPM8 by inflammatory mediators in HEK293 cells (a, b) or $G\alpha_{q/11}^{-/-}$ MEF cells (c, d) co-expressing B2R (a, c) or H1R (b, d). Same cell types as used in experiments in Fig. 2e, 2g, 5e and 5c, respectively. **(a)** TRPM8 current evoked by a voltage ramp (-120mV to +160mV, 650ms) was inhibited by BK (1mM), and the inhibition was not blocked by 2.5mM U73122 (blue trace). **(b)** Similar experiment with histamine (10mM). In this case the inhibition caused by histamine (blue curve) was partially reversed by U73122 (dark red curve). **(c, d)** Bradykinin (1mM) and histamine (10mM) have little effect on voltage-induced TRPM8 activation in $G\alpha_{q/11}^{-/-}$ MEF cells; however, bradykinin and histamine caused a large inhibition of TRPM8 after co-transfection of the $3G\alpha_{qiq}$ chimera, which does not couple to PLCb.

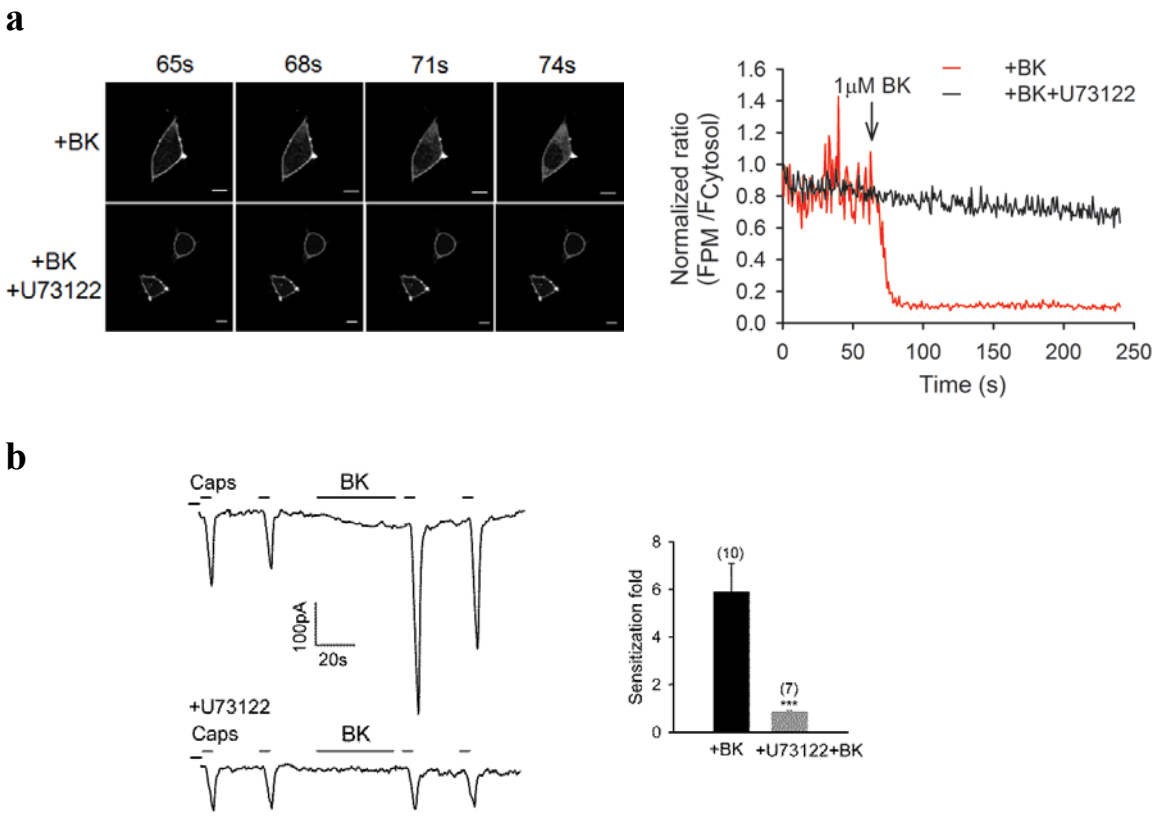

Figure S3 U73122 completely blocks BK-induced PIP_2 hydrolysis and functional sensitization of TRPV1 by BK. **(a)** HEK293 cells transfected with the bradykinin receptor B2R and Tubby-cYFP-R322H were live imaged. 1mM BK added at 65s, and Tubby translocation was observed within 10s (upper panels). U73122 (2.5mM) pre-treatment for 5 minutes completely blocked Tubby translocation (lower panels). Scale bar 10mM. Graph on right gives quantification of ratio of membrane fluorescence to that of cytosol as a function of time in the cells shown left. Arrow indicates addition of 1mM BK. **(b)** BK (1mM) sensitized TRPV1 inward current activated by 10nM capsaicin in a HEK293 cell expressing TRPV1 and B2R (top trace). U73122 (2.5mM, bottom trace) completely blocked sensitization. Zero currents indicated at left. On right is summary of similar experiments. Number of cells given above each bar, data are mean ± SEM. ***P<0.001.

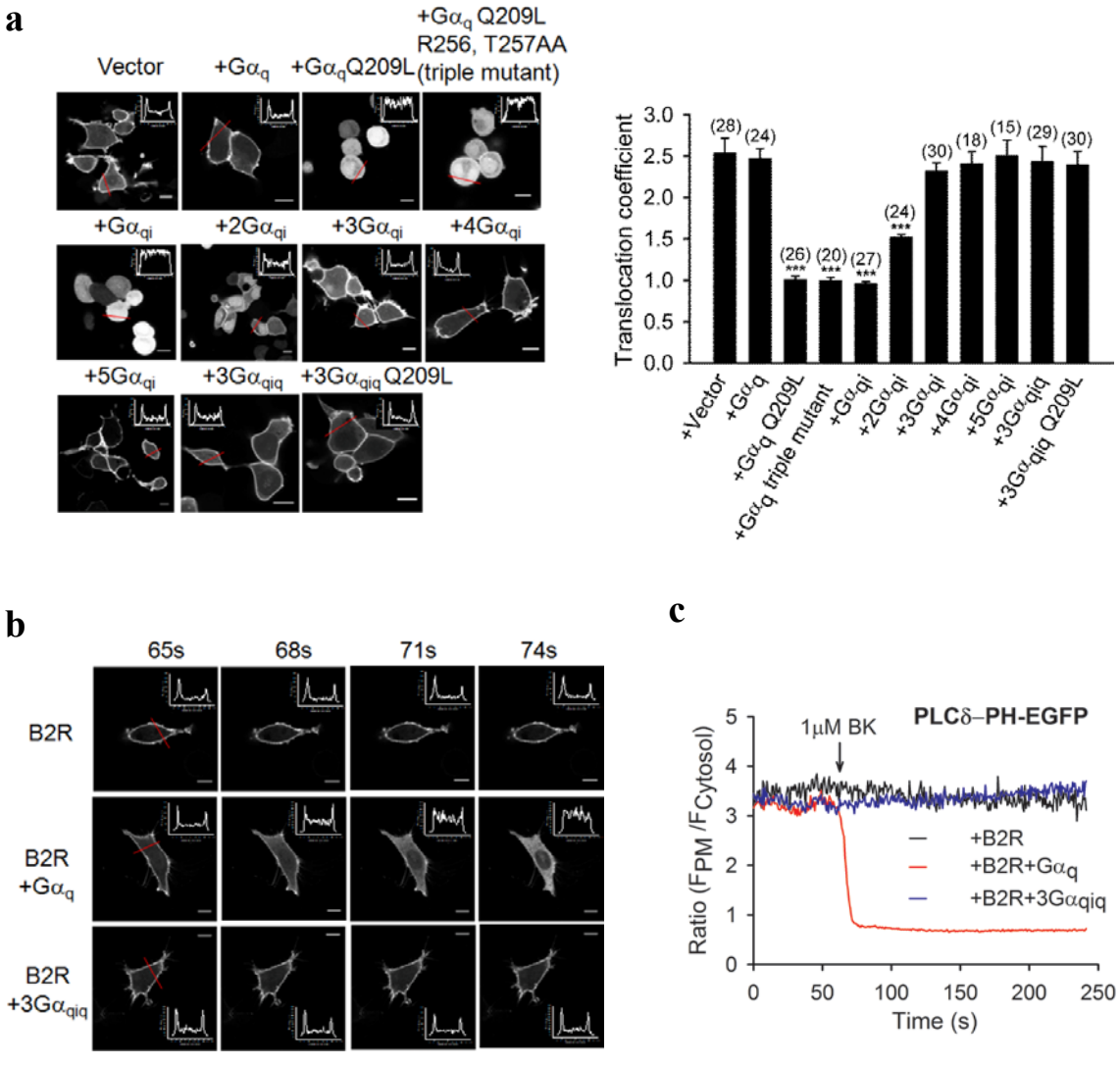

Figure S4 The effect of Ga_q chimeras on Tubby-cYFP-R332H and PLCd-PH-EGFP localization and PIP_2 hydrolysis. **(a)** Typical example images of Tubby-cYFP-R332H in HEK293 cells co-transfected with different Ga_q chimeras as indicated. Profiles of intensity across cells (indicated by red line) shown inset at top corner of the images. Ga_q Q209L, Ga_q Q209L/R256A/T257A, Ga_{qi} and $2G\alpha_{qi}$ caused PIP2 depletion and Tubby translocation, while all other chimeras lost the ability to deplete PIP2 and so to translocate the Tubby probe. Scale bar 10mM. On right is the summary of quantification of translocation coefficient (ratio of membrane peak fluorescence to that of mean fluorescence in the cytosol in line profile intensity) for each G protein. Number of cells given above each bar. Bars are mean±SEM. ***P<0.001. **(b)** Translocation of PLCd-PH-EGFP induced by BK in $G\alpha_{q/11}^{-/-}$MEF cells co-transfected with B2R and G proteins as indicated. 1mM BK was added at 65s. Scale bar 10μm. Profiles of intensity across cells (indicated by red line) shown inset at corner of the images. **(c)** Quantification of relative membrane Tubby fluorescence signal as a function of time in b. Each experiment repeated at least 4 times with similar results.

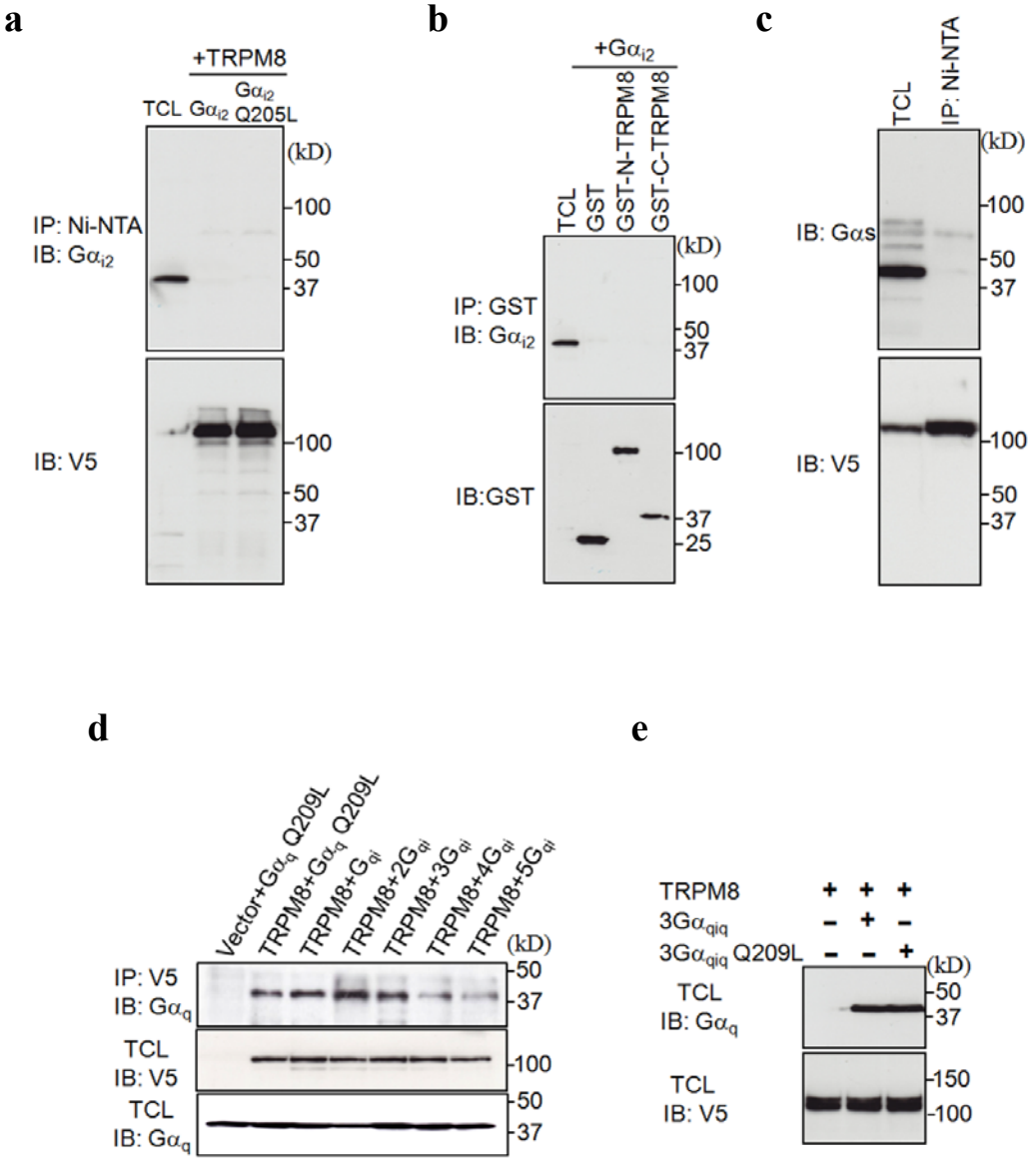

Figure S5 Interaction of TRPM8 with Ga protein subunits and $G\alpha_q$ chimeras. **(a)** TRPM8 shows no significant binding to $G\alpha_{i2}$. Experiments carried out under same conditions that had shown binding of $G\alpha_q$ to TRPM8 (see Fig. 6a-d). TRPM8 pulled down by Ni-NTA beads from HEK293 cells expressing TRPM8-V5-His and $G\alpha_{i2}$, and probed with anti-$G\alpha_{i2}$ (top blot) followed by detection of TRPM8 in stripped blot with anti-V5 (bottom blot). First lane is total cell lysate (TCL); last two lanes are pull down samples. Molecular weight shown on right, same for all other blots. **(b)** GST-coupled TRPM8 N and C terminals used to pull down $G\alpha_{i2}$ in experiments similar to those in Fig. 6d. No significant binding to $G\alpha_{i2}$ found. **(c)** TRPM8 shows no significant binding to $G\alpha_s$. TRPM8 was pulled down from HEK293 cell lysate expressing TRPM8-V5-His and $G\alpha_s$. $G\alpha_s$ detected by anti-$G\alpha_s$ (top blot) followed by anti-V5 for TRPM8 (bottom blot). No significant association found. **(d)** Interaction of TRPM8 with different $G\alpha_q$ chimeras. TRPM8 was immunoprecipitated by anti-V5 from lysate of HEK293 cells expressing TRPM8-V5 together with different $G\alpha_q$ chimeras. Co-precipitated $G\alpha_q$ chimeras were probed by anti-$G\alpha_q$ antibody (top blot). Expression of TRPM8 and $G\alpha_q$ in total cell lysate (TCL) for each sample was detected by anti-V5 (middle blot) and anti-$G\alpha_q$ (bottom blot), and was similar in all cases. **(e)** $3G\alpha_{qiq}$ chimera and Q209L mutant do not affect TRPM8 expression. HEK293 cells co-transfected with cDNAs as indicated, expression of $3G\alpha_{qiq}$ chimera and TRPM8 protein detected by anti-$G\alpha_q$ (top blot) and anti-V5(bottom blot), respectively.

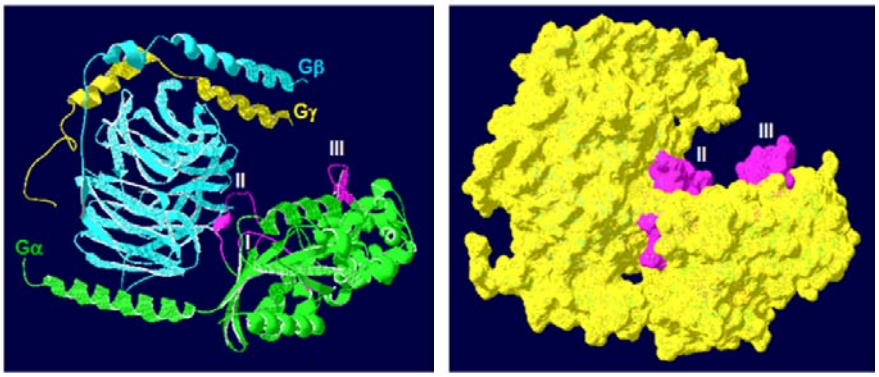

Figure S6 Structure of $G\alpha_q\beta g$ modelled by homology modelling based on the crystallized structure of $G\alpha_i\beta g$ (Protein Data Bank code, 1GG2)[1] by using Swiss-Pdb viewer 4.0 software together with Swiss online modelling software. $G\alpha_q$ protein in green, Gb in blue and Gg in yellow. Switch I, II and III regions of $G\alpha_q$ in pink. On right is molecular surface representation. Surfaces of Switch II and III regions shown in pink. Surface of Switch I region is at the back and cannot be seen in these orientations. Switch III region is largely free to be accessed by effectors and is identified as the TRPM8 binding region (see Fig.6f). The activated form of $G\alpha_q$ has a similar structure in the Switch III region[2] (Protein Data Bank code, 2BCJ), which would also be free to engage TRPM8. Thus based on our current knowledge of the structure of $G\alpha_q$, the Switch III region is available to be accessed and engaged by effectors such as TRPM8 in both the active and inactive configurations.

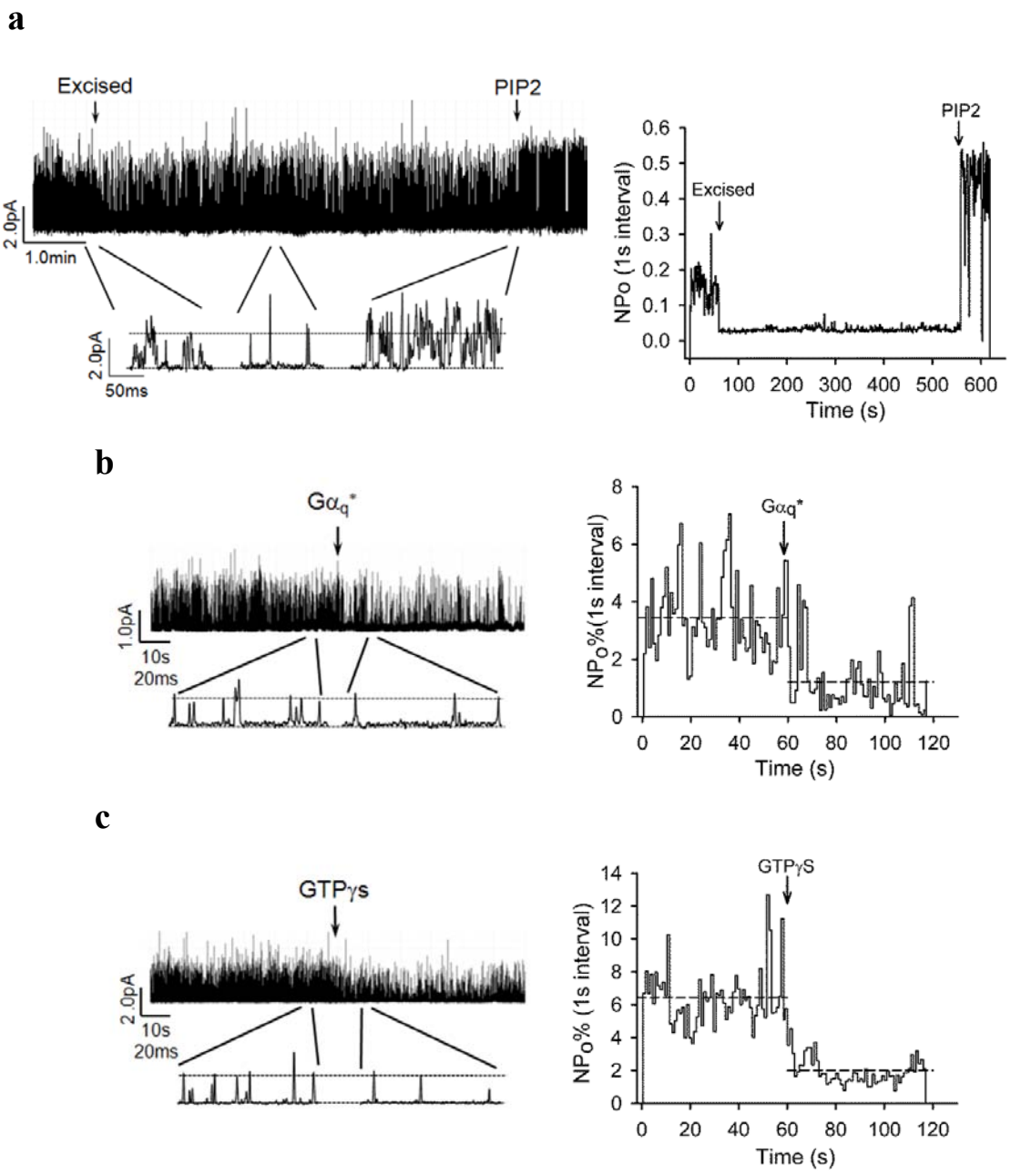

Figure S7 Effect of DiC8-PIP_2, activated $G\alpha_q$ and GTPγS on TRPM8 channels excised from HEK293 cells expressing TRPM8. **(a)** Example trace of TRPM8 channel activity (+40mV) in cell attached mode, following excision and with addition of DiC8-PIP_2 (50mM), as indicated by arrows. Sections of traces shown below at higher time resolution. Right: real time quantification of NP_o. On cell NP_o = 0.15±0.0054; after excision NP_o = 0.032±0.00028; after DiC8-PIP_2 addition NP_o = 0.43±0.015. TRPM8 channels typically maintain constant low level of activity over 6 mins following excision. **(b, c)** Left: typical examples of channel activity at +40mV in already run-down patches excised from HEK cells expressing TRPM8 after addition of 50nM $G\alpha_q$* ($G\alpha_q$ pre-incubated with GTPγS, b) or 100mM GTPγS (c). Arrows indicate time of addition of $G\alpha_q$* or GTPγS. Sections of traces are shown below at higher time resolution. Right: real time quantification of NP_o; dashed lines give mean NP_o over indicated time periods. NP_o before $G\alpha_q$*, 0.034 ± 0.0018; after $G\alpha_q$*, 0.012 ± 0.0016; P<0.001. NP_o before GTPγS, 0.064±0.0022; after GTPγS, 0.02 ± 0.0012; P<0.001.

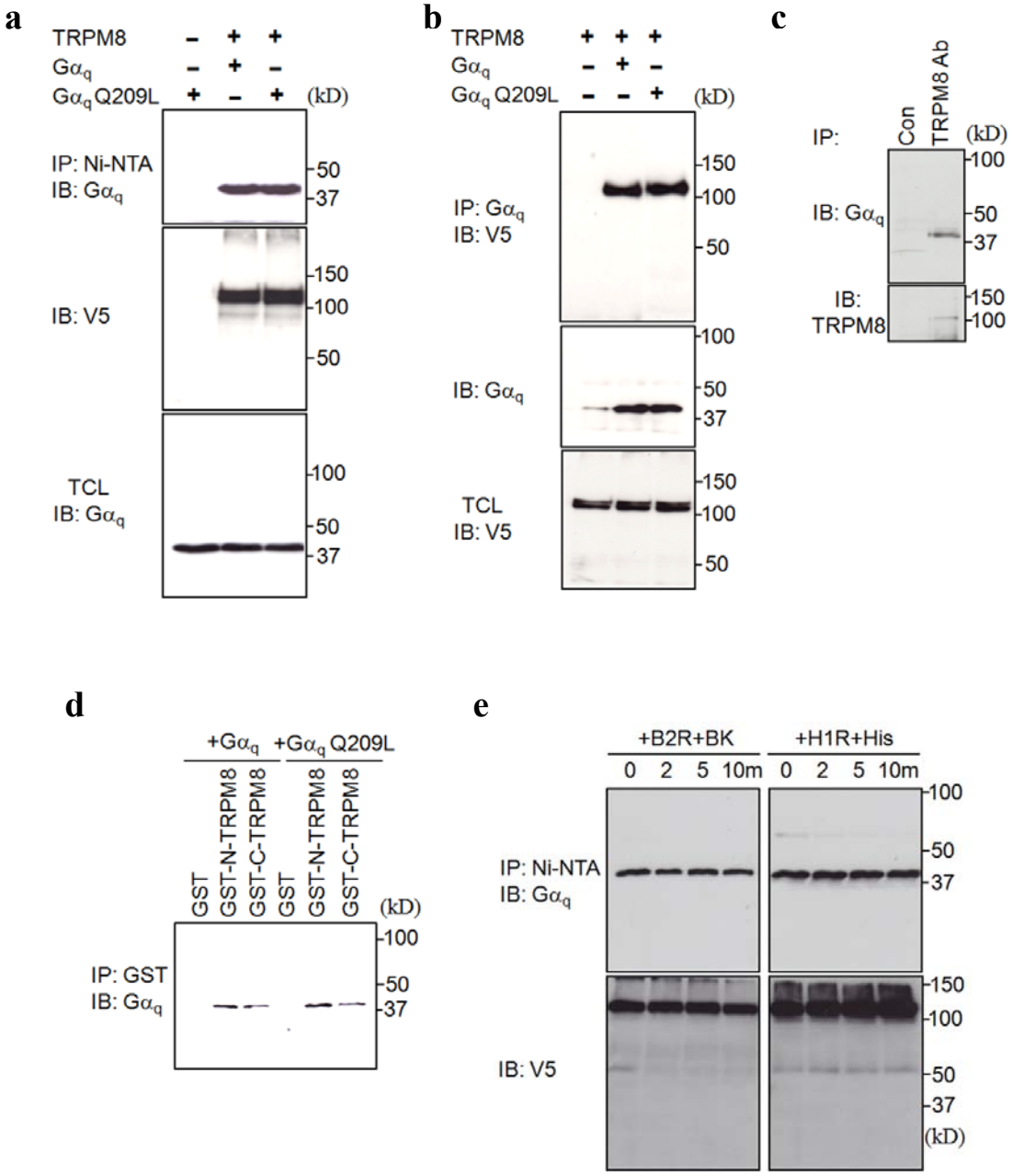

Figure S8 Full scan images of blots of Figure 6. **(a)** Fig.6a. **(b)** Fig. 6b. **(c)** Fig. 6c. **(d)** Fig.6d. **(e)** Fig. 6e.

References

1. Wall, M.A. *et al.* The structure of the G protein heterotrimer Gi alpha 1 beta 1 gamma 2. *Cell* **83,** 1047-1058 (1995).

2. Tesmer, V.M., Kawano, T., Shankaranarayanan, A., Kozasa, T., & Tesmer, J.J. Snapshot of activated G proteins at the membrane: the Galphaq-GRK2-Gbetagamma complex. *Science* **310,** 1686-1690 (2005).